

RESEARCH ARTICLE

Toxicity and inflammatory potential of mineral fibres: The contribute of released soluble metals versus cell contact direct effects

Vanessa Almonti^{1,2} | Stefania Vernazza^{1,2} | Serena Mirata^{1,2}  | Sara Tirendi^{1,2} |
Mario Passalacqua^{1,2} | Alessandro Francesco Gualtieri³ | Dario Di Giuseppe³ |
Sonia Scarfi^{2,4}  | Anna Maria Bassi^{1,2}

¹Department Experimental Medicine,
University of Genova, Genova, Italy

²Inter-University Center for the Promotion of
the 3Rs Principles in Teaching & Research
(Centro 3R), Pisa, Italy

³Department of Chemical and Geological
Sciences, University of Modena and Reggio
Emilia, Modena, Italy

⁴Department Earth, Environment and Life
Sciences, University of Genova, Genova, Italy

Correspondence

Sonia Scarfi, Inter-University Center for the
Promotion of the 3Rs Principles in Teaching &
Research (Centro 3R), 56122 Pisa, Italy.
Email: soniascarfi@unige.it

Funding information

PRIN-Bando 2017-Prot.20173 x 8WA4

Abstract

Asbestos fibres have been considered an environmental hazard for decades. However, little is known about the attempts of circulating immune cells to counteract their toxicity. We addressed the early effects of fibre-released soluble factors (i.e. heavy metals) in naïve immune cells, circulating immediately below the alveolar/endothelial cell layer. By comparison, the direct fibre effects on endothelial cells were also studied since these cells are known to sustain inflammatory processes. The three mineral fibres analysed showed that mainly chrysotile (CHR) and erionite (ERI) were able to release toxic metals in extracellular media respect to crocidolite (CRO), during the first 24 h. Nevertheless, all three fibres were able to induce oxidative stress and genotoxic damage in indirectly challenged naïve THP-1 monocytes (separated by a membrane). Conversely, only CHR-released metal ions induced apoptosis, NF- κ B activation, cytokines and CD163 gene overexpression, indicating a differentiation towards the M0 macrophage phenotype. On the other hand, all three mineral fibres in direct contact with HECV endothelial cells showed cytotoxic, genotoxic and apoptotic effects, cytokines and ICAM-I overexpression, indicating the ability of these cells to promote an inflammatory environment in the lung independently from the type of inhaled fibre. Our study highlights the different cellular responses to mineral fibres resulting from both the nature of the cells and their function, but also from the chemical-physical characteristics of the fibres. In conclusion, CHR represented the main pro-inflammatory trigger, able to recruit and activate circulating naïve monocytes, through its released metals, already in the first 24 h after inhalation.

KEYWORDS

asbestos fibres, carcinogenicity, in vitro model, toxicity, zeolite

Vanessa Almonti and Stefania Vernazza should be considered joint first authors.

Sonia Scarfi and Anna Maria Bassi should be considered joint senior authors.

1 | INTRODUCTION

Asbestos minerals and zeolite erionite fibres are considered the most relevant and widespread natural-occurring mineral species (Gualtieri, 2023). According to the World Health Organisation (WHO) and the International Agency for Research on Cancer (IARC), these fibres represent environmental and occupational hazards since they can cause cancer in humans (IARC, 2012; WHO, 2014; Sarkar Phyllis et al., 2021) due to their physical–chemical-specific properties (i.e. morphology, surface activity, bio-durability and iron content).

The generic term ‘asbestos’ identifies two categories of minerals with a fibrous-asbestiform crystal habit: amphibole and serpentine. In these categories, six mineral species are included: chrysotile, the only serpentine type and five fibrous amphiboles, which are amosite, crocidolite, anthophyllite, tremolite and actinolite (Gualtieri, 2023). Erionite is a fibrous zeolite that may exhibit an asbestiform crystal habit, classified as a series including three different species, that is, erionite-Ca, erionite-Na or erionite-K, based on the predominant cation in the chemical composition (Ballirano et al., 2017; Gualtieri, 2023). Natural fibrous erionite is carcinogenic and, as an environmental contaminant, has recently caused great concern because its presence in breathing air has been linked to the outbreak of malignant mesothelioma (MM) (Carbone et al., 2011; Ilgren et al., 2008).

Although several epidemiological studies have reported that long-term inhalation of airborne asbestos fibres results in chronic lung inflammation and well-documented pulmonary diseases (Dalsgaard et al., 2021; Gualtieri, 2023; Gualtieri et al., 2019; Manning et al., 2002), the WHO has not yet formally established the minimum asbestos exposure threshold causing carcinogenesis, also because, as it is known, asbestos-related tumours (i.e. lung carcinomas, MM) have a long latency period (Nicolini et al., 2020; Røe & Stella, 2015). Moreover, to date, only amphibole asbestos minerals are banned worldwide, while chrysotile is banned in 67 countries, with the exception of China, India, Kazakhstan and Russia (Baur & Frank, 2021; Frank, 2020). This distinction arises from the fact that the low bio-persistence of chrysotile in the human body makes it seemingly less toxic to human health compared to amphiboles (Gualtieri, 2021, 2023). In this regard, a recent animal study revealed systemic effects, including marked neutrophilia, prolonged inflammation, microgranulomas and fibrosis, together with an increased susceptibility to cancer, after the chronic inhalation (for a period of 90 days) of brake dust containing amphibole fibres, but not with the inhalation of the same dust in the presence of chrysotile fibres (Bernstein et al., 2021). Nevertheless, in the light of the differences between human and animal physiology, as confirmed by the authors of the study, it is necessary to also consider the relevance of such a study on human models.

This study aimed at analysing three well-known mineral fibres on two different *in vitro* human models consisting of a monocyte-like cell line (THP-1) and the human endothelial vein cell line (HECV). The first cellular model is considered a valuable tool for investigating monocyte responses to stressors in both health and disease (Bosshart &

Heinzelmann, 2016). Conversely, the second model represents the vascular endothelium lining in alveolar capillaries and constitutes the initial barrier to circulating inflammatory and immune naïve effector cells, which are recruited in response to insults to the lung (Garcia et al., 1988). Therefore, to better mimic the lung microenvironment *in vivo*, where inactive circulating monocytes can be activated towards the macrophage phenotype by a stressful stimulus and act as effector cells together with the pulmonary endothelium, human THP-1 monocytes together with HECV human venous endothelial cells were used as cellular models due to their crucial role in triggering inflammatory processes, participating in fibre phagocytosis, and in cellular damage responses (Garcia et al., 1988; Jakubzick et al., 2013; Richter et al., 2016).

Since monocytes are circulating cells in the alveolar capillaries and as such they rarely would come to direct contact with the mineral fibres, we studied several early adverse cellular effects on THP-1 cells during indirect contact with standard crocidolite UICC (CRO), a chrysotile (CHR) from the Balangero mine (Italy) and a fibrous erionite (ERI) from Jersey (USA) by means of physical separation through a semipermeable membrane insert containing the fibres. By this approach we addressed the early effects of fibre-released soluble factors (i.e. heavy metals, ions, toxic impurities) eventually able to cause cell damage and/or pro-inflammatory effects in naïve immune cells, circulating immediately below the alveolar/endothelial cell layer. This is an issue that, relatively to mineral fibres, has until now not been properly investigated. We also investigated the direct effects caused by the same fibres on the endothelial cells to set up an *in vitro* model better simulating the *in vivo* microenvironment. Initially, the metal released by CRO, CHR and ERI fibre leakage was evaluated in culture media at a physiological pH (7.4). Then, cell responses from the indirect and direct experimental treatments on THP-1 and HECV were analysed in terms of cytotoxicity, genotoxicity and pro-inflammatory potential. From these evaluations, we tried to infer how these under-investigated effects may have a relationship with the toxic and carcinogenic capacity of the mineral fibres.

2 | MATERIALS AND METHODS

2.1 | Cell cultures

Human leukaemia monocytic cell line (THP-1) was obtained from the Biological Bank and Cell Factory (IRCCS AOU San Martino-IST, Italy) and cultured in standard culture conditions (37°C and 5% CO₂) with RPMI-1640 (Euroclone®, Italy), supplemented with 10% (v/v) FBS (Euroclone®), 2 mM L-glutamine (Euroclone®), 1% penicillin/streptomycin (Corning Inc, USA). THP-1 cells were sub-cultured every 3–4 days when the cell density exceeded 1×10^6 cells/ml.

All cultures were found to be mycoplasma-free during regular checks with the Reagent Set Mycoplasma Euroclone (Euroclone®). For experimental procedures THP-1 were seeded at 1×10^6 , 1.5×10^5 and 5×10^4 cells/well, respectively, in 6-, 12- and 24-well plates.

Human umbilical vein endothelial cells (HECV) derived from human umbilical cord of a Caucasian subject were obtained from Biological Bank and Cell Factory (IRCCS AOU San Martino-IST) and cultured with DMEM (Euroclone®), supplemented with 10% (v/v) FBS, 2 mM L-glutamine, 1% penicillin/streptomycin, in standard culture conditions (37°C and 5% CO₂). Cells were split up at 70% confluence with 2 ml of TrypLE™ Express (TEX) (Invitrogen Life Technologies, Waltham, USA); then TEX was blocked with double volume of supplemented culture medium. For experimental procedures, HECV were seeded at 5×10^5 , 1×10^5 and 1×10^4 cells/well, respectively, in 6-, 24- and 96-well plates.

2.2 | Crocidolite, chrysotile and erionite fibre suspensions

The mineral fibres investigated were (i) UICC standard crocidolite (South Africa, NB #4173-111-3), abbreviated CRO; (ii) chrysotile from Balangero (Turin, Italy), abbreviated CHR; and (iii) erionite-Na fibrous from Jersey (Nevada, USA), abbreviated ERI. Selected chemical and physical data of these fibres are briefly reported in Table 1. Detailed information concerning the samples can be found in Gualtieri et al. (2016), Pollastri et al. (2016) and Pacella et al. (2019). For detailed information on the crystalline structure of mineral fibres, the reader can refer to the work of Ballirano et al. (2017). The morphological and morphometric characteristics of the fibres are described in detail in Di Giuseppe et al. (2022). SEM analyses were performed using a FEI Nova NanoSEM 450 FEG-SEM equipped with an energy-dispersive x-ray (EDX) spectrometer (Bruker QUANTAX-200). Data were recorded using an accelerating voltage of 15 kV and a beam current of 3.5 µA.

For the cell experiments, fibre suspensions were prepared as follows: After autoclave sterilisation, 5 mg of each fibre (CRO, CHR, and ERI) was suspended in 1 ml of phosphate-buffered saline (PBS) (Euroclone®) and sonicated to separate the fibres in a smaller size; these stock suspensions were stored at –20°C until use.

Before proceeding with the experimental treatments, each fibre stock solution was further sonicated, and 50 µg/ml fibre (w/v) was added into the culture medium according to previous studies (Broaddus et al., 1997; Fenoglio, Croce, et al., 2000; Fenoglio, Fubini, et al., 2000; Hamilton et al., 1996; Ollikainen et al., 1999; Puhakka et al., 2002).

2.3 | Trace metal quantification in culture medium

Quantification of the metal ions released into the culture medium from the fibres was assessed in acellular conditions. Briefly, 50 µg/ml of the three mineral fibres suspended in RPMI complete medium was incubated for 24 h at 37°C. Then, 100 µl of 1 M perchloric acid (PCA) (Sigma-Aldrich, Milan, Italy) was added to the fibre-containing media, and the samples were centrifuged at $3220 \times g$ for 10 min to pellet the fibres and the precipitated proteins. The

TABLE 1 Characteristics of the analysed mineral fibres.

Sample	Provenance	Mean fibre length and width (µm) (Di Giuseppe et al., 2022)	Fe ²⁺ (wt%)	Fe ³⁺ (wt%)	Ni (ppm) (Bloise et al., 2016)	Co (ppm) (Bloise et al., 2016)	Cr (ppm) (Bloise et al., 2016)	In vitro biodegradability (y) (Gualtieri et al., 2018)	References
Crocidolite (CRO) (Na _{1.96} Ca _{0.03} K _{0.01})(Fe ²⁺ _{2.34} Fe ³⁺ _{2.05} Mg _{0.52})(Si _{7.84} Al _{0.02})O _{21.36} (OH) _{2.64}	Northern Cape (South Africa) ^a	L: 16 W: 0.64	13.5	12.5	13.2	1.62	19.7	66(16)	Bloise et al. (2016) Pacella et al. (2019)
Chrysotile (CHR) Mg _{5.81} Fe ²⁺ _{0.15} Al _{0.27} Fe ³⁺ _{0.09} Cr _{0.01} (OH) _{7.11} Si _{3.97} O ₁₀	Balangero, Turin (Italy)	L: 35 W: 0.59	1.94	0.28	446	40.4	>1000	0.3(1)	Pollastri et al. (2016)
Erionite (ERI) (Na _{5.35} K _{2.19} Ca _{0.15} Mg _{0.11} Ti _{0.05})[Si _{28.01} Al _{7.90} O ₇₂]-28.1 H ₂ O	Jersey, NE (USA)	L: 9.4 W: 0.55	–	0.55	1.72	0.78	1.7	181(68)	Gualtieri et al. (2016)

^a UICC standard Crocidolite NB #4173-111-3.

supernatants were then collected and diluted in distilled water (1:5) before proceeding with the analysis of metals (Al, Mg, Fe, Ni, Co and Cr) released into the medium. The metals were detected by a Scientific iCAP™ TQ inductively coupled plasma-mass spectrometer (ICP-MS) and analysed by TQ-O2 and SQ-KED measurement modes (Thyssen et al., 2018). Technical details about the analysis procedure can be found in Mirata et al. (2022).

2.4 | Indirect THP-1 and direct HECV cell exposure to the fibres

THP-1 cells were indirectly exposed to 50 µg/ml of CRO, CHR and ERI suspensions by using the cell inserts equipped with ThinCert® porous membrane (0.4 µm diameter) (Greiner Bio-One S.r.l., Italy). THP-1 cells were seeded into multi-well cell plates containing porous membrane inserts on which the fibre suspensions were added. The physical separation between the solution containing the mineral fibres and the THP-1 cells allowed studying potential toxic effects induced by any metals/ions released by the fibres.

The direct exposure to HECV cells was conducted at a fibre concentration of 50 µg/ml.

2.5 | DCF assay

The production of reactive oxygen species (ROS) from THP-1 cells was monitored by dichlorofluorescein (DCF) assay after 4- and 24-h indirect exposure to the fibre solutions. Before proceeding with the experimental treatments, THP-1 cells were pre-treated with non-fluorescent 2',7'-dichlorodihydrofluorescein diacetate (H₂DCFDA, Life Technologies, USA) that freely permeates the plasma membrane and is reduced to the highly fluorescent DCF (Wang & Joseph, 1999). Briefly, after removing the culture medium by centrifugation (at 90 × g for 5 min), the pellet of THP-1 was rinsed with Hank's balanced salt solution Ca⁺, Mg⁺ (HBSS, Life Technologies) and incubated with 10 µM H₂DCFDA in HBSS at 37°C in 5% CO₂ for 45 min in a test tube. Then, after removing the H₂DCFDA solution, the THP-1 cells were washed in HBSS, suspended in culture medium and seeded into 24-well plates (5 × 10⁴ cells/well) to be submitted to indirect exposure for 4 and 24 h to CRO, CHR and ERI solutions. At each experimental time, the inserts were removed, and DCF detection was carried out on a fluorescent plate reader (CLARIOstar, BMG LABTECH, Germany), with excitation and emission wavelengths of 485 and 520 nm, respectively.

The oxidative stress in HECV cells was observed after 4-h direct exposure to the fibres into 96-well plates. First, after removing the HECV medium, the cells were washed with HBSS and incubated with 10 µM H₂DCFDA in HBSS at 37°C in 5% CO₂ for 45 min. Then, after removing the dye solution, the HECV cells were washed in HBSS and directly treated with fibre solutions for 4 h. The fluorescence was read at the end of the exposure time. The fluorescence intensity was

expressed as a percentage of relative fluorescence unit of treated versus untreated THP-1 and HECV cells.

2.6 | Proliferation assay

The THP-1 and HECV proliferation was measured in terms of DNA content according to Rao and Otto (1992) after 24, 48 and 72 h of experimental conditions. 1.5 × 10⁵ THP-1 cells were seeded in a 12-multi-well cell plate and submitted to indirect exposure to the three fibre suspensions, as described above. At the end of each experimental treatment, the cell medium was collected, centrifuged at 90 × g for 5 min to recover non-adherent cells, and after removing supernatant, 1 ml of lysis solution (urea 10 M, 0.01% SDS in saline sodium citrate buffer [SSC], 0.154 M of NaCl, 0.015 M of Na₃ citrate, pH 7) (Sigma-Aldrich) was added to the cellular pellet. The same lysate solution was put on the well to harvest the remaining adherent cells. Then, the dissolved cell suspensions were incubated at 37°C in a shaking bath for 2 h, and 1 ml of Hoechst 33258 dye (Sigma-Aldrich) (1 µg/ml in SSC buffer) was added in the dark.

1 × 10⁵ HECV cells were seeded in a 24-well plate, and at the end of the exposure time with the mineral fibres, the experimental treatment was removed. After three rinses with HBSS, 1 ml of lysis solution was added to each well to dissolve cell monolayers. The obtained cell suspensions were then incubated at 37°C in a shaking bath for 2 h, and at the end, 1 ml of Hoechst 33258 dye (1 µg/ml in SSC buffer) was added in the dark.

The absorbance was measured with CLARIOstar (BMG LABTECH, Germany) at excitation and emission wavelengths of 355 and 460 nm, respectively. The cell proliferation was estimated by referring fluorescence units to a linear standard curve of DNA fluorescence versus cell number. The results are the mean of two experiments performed in triplicate.

2.7 | Apoptosis death rate by confocal microscopy

The cell apoptosis was assessed by confocal microscopy analyses using a Nikon AX R confocal microscope equipped with a 60× NA 1.42 objective (Nikon Europe, Amstelveen, The Netherlands). THP-1 monocytes were indirectly treated with the three mineral fibres in 12-well plates equipped with ThinCert® porous membrane for 24 h, and, at the end of the experimental time, they were collected by centrifugation. HECV were directly treated in a µ-Slide eight-well high ibiTreat (Ibidi®, Gräfelfing, Germany) at 3 × 10⁴ cells/well. Both cell types were stained with Annexin V, FITC Apoptosis Detection Kit (Dojindo EU, Munich, GmbH) following the manufacturer's instructions. The acquired images were then obtained in phase-contrast mode and in fluorescence mode, acquiring the green fluorescence of annexin-positive cells and the red fluorescence of propidium iodide-positive cells (emission range of 500–550 nm and 600–670 nm, respectively) in single stacks.

2.8 | Gene expression analyses

To verify if following 24-h indirect exposure to the investigated fibres, the THP-1 cells were able to start a differentiation towards a macrophage M0 phenotype and triggered an early pro-inflammatory response, the gene expression of CD163 and CXCL10 differentiation markers was measured by qPCR. The IL-1 β , IL-6, TNF- α , IL-8 and MCP-1 cytokine gene levels were also evaluated in both THP-1 and HECV cells after 24 h of indirect and direct treatment, respectively. Moreover, the same analysis in HECV cells measured the gene expression of VEGF and ICAM-1 as markers of endothelial growth and inflammatory activation. Briefly, total RNA was extracted using the NucleoSpin RNA, Mini kit (MACHEREY-NAGEL, Dueren, Germany) according to the manufacturer's instructions. The quality and quantity of the RNA were analysed using a NanoDrop spectrophotometer (NanoDrop Technologies, USA), and then the cDNA (1 μ g per sample) was synthesised by using a cDNA Synthesis Kit (biotechrabbit GmbH, Henningsdorf, Germany). Each PCR reaction was performed in 10 μ l containing: 4 \times master mix (biotechrabbit GmbH), 0.2 μ M of each primer and 1 ng of synthesised cDNA. All samples were analysed in triplicate. The following thermal conditions were used: initial denaturation at 95°C for 3 min, followed by 45 cycles with denaturation at 95°C for 15 s, annealing and elongation at 60°C for 60 s. The fluorescence was measured at the end of each elongation step. The next step was a slow heating (1°C/s) of the amplified product from 55 to 92°C to generate a melting temperature curve. Values were normalised to HPRT-1 (housekeeping gene, a.n. NM_000194.3) mRNA expression for THP-1 naïve monocytes, while they were normalised to GAPDH (housekeeping gene, a.n. NM_002046) mRNA expression for HECV endotheliocytes. All primers (Table 2) were designed using the Beacon Designer 7.0 software (Premier Biosoft International, USA) and obtained from TIB MOLBIOL (Genoa, Italy). Data analyses were obtained using the DNA Engine Opticon[®] 3 Real-Time Detection System Software program (3.03 version). To calculate the relative gene expression compared to an untreated (control) calibrator sample, the comparative threshold Ct method (Aarskog & Vedeler, 2000) was used within the Gene

Expression Analysis for iCyclerIQ™ Real-Time Detection System software (Vandesompele et al., 2002).

2.9 | Cytokine release by enzyme-linked immunosorbent assay (ELISA)

The pro-inflammatory process was evaluated by the release of IL-1 β and TNF- α cytokines in both indirectly treated THP-1 and directly treated HECV cell media for 24 h. The cytokine content was measured by ELISA kits (human IL-1beta ELISA kit and TNF-alpha human ELISA kit, respectively, Abcam, UK) following the manufacturer's instruction.

2.10 | Western blot analyses

The whole THP-1 cell lysates were collected after 24 hr of indirect fibre exposure into six-well plates to detect pro-inflammatory and genotoxic effects as NF- κ B and γ -H2AX protein signals. Conversely, HECV protein samples were collected at two different exposure times, 6 and 24 h, to observe the pro-inflammatory activation and genotoxic damage respectively, of direct fibre treatments into six-well plates. 250 μ l of ice-cold RIPA lysis buffer (Sigma Aldrich, USA) plus protease inhibitor cocktail (Complete Tablets, Roche Diagnostic GmbH, Germany) was added to the cell pellets previously washed with PBS. The cells were then sonicated three times for 15 s and centrifuged at 4°C for 15 min at 14,000 \times g. Supernatants were transferred to a fresh tube, and the protein concentration of each cell lysate was determined. Thus, 30 μ g of proteins were added to 4X Laemmli buffer (Bio-Rad Laboratories, Inc., USA), and the samples were reduced and denatured by boiling lysates at 99°C for 5 min. The samples were loaded into pre-made gel 4%–20% Mini-PROTEAN TGX Precast Protein Gels (Bio-Rad Laboratories) in SDS-PAGE Running Buffer and transferred onto PVDF membrane (Thermo Scientific, USA) and probed with specific primary antibodies against rabbit phospho-NF- κ B p65, Ser 536 (Cell Signalling Technology, USA), rabbit NF- κ B p65 (Cell Signaling Technology), rabbit Anti-H2AX

TABLE 2 List of primer pairs used for qPCR experiments in THP-1 human monocytes.

Gene	GenBank (a.n.)	Forward	Reverse	Size (bp)
CD163	NM_004244.5	GTCGCTCATCCCGTCAGTCATC	GCCGCTGTCTCTGTCTTCGC	114
CXCL10	NM_001565.4	GAAAGCAGTTAGCAAGGAAAGGTC	ATGTAGGGAAGTGATGGGAGAGG	120
IL-1 β	NM_000576.3	TGATGGCTTATTACAGTGGCAATG	GTAGTGGTGGTCGGAGATTCG	140
IL-6	NM_001318095.2	CAGATTTGAGAGTAGTGAGGAAC	CGCAGAATGAGATGAGTTGTC	194
TNF- α	NM_000594.4	GTGAGGAGGACGAACATC	GAGCCAGAAGAGGTTGAG	113
IL-8	NM_000584.4	AATTCATTCTCTGTGGTATC	CCAGGAATCTTGATTGC	127
MCP-1	NM_002982	CTTCTGTGCCTGCTGCTC	CTTGCTGCTGGTGATTCTTC	156
VEGF	NM_001025370.1	TTCGGGCTGTTCTCGCTTC	CTCTCCTTCTCTCTCTCTCC	142
ICAM-1	NM_000201.2	CAACCGGAAGGTGTATGAAC	CGAGGTGTTCTCAAACAGCTC	390
HPRT-1	NM_000194.3	GGTCAGGCAGTATAATCCAAAG	TTCATTATAGTCAAGGGCATATCC	144
GAPDH	NM_002046	CCTGTTCGACAGTCAGCCG	CGACCAAATCCGTTGACTCC	100

(Abcam, UK), mouse Anti-phospho-Ser139 gamma H2AX (Abcam, UK) and mouse GAPDH (Santa Cruz Biotechnology, USA) followed by incubation with HRP-conjugated secondary antibodies (NA9340V and NA931V, against rabbit and mouse primary antibodies, respectively, Amersham Life Science, Italy). The proteins were detected by Western Bright™ ECL (Advansta, USA), exposed to film and analysed using a BIORAD Gel Doc 2000. Densitometrical data obtained from Quantity One software (Bio-Rad Laboratories) were applied for statistical analysis and normalised against the housekeeping GAPDH. The results were expressed as fold versus untreated cultures, respectively.

2.11 | Genotoxic damage by confocal microscopy analysis

Phospho-H2AX (γ -H2AX) foci—bright dots—in the nucleus were analysed after 24 h of fibre treatment on THP-1 and HECV cells by confocal microscopy. 1×10^6 THP-1 cells were seeded into six-well plates and indirectly exposed to the CRO, CHR and ERI (50 $\mu\text{g}/\text{ml}$) by the presence of the membranous inserts. On the other hand, 3×10^4 HECV cells were seeded in μ -Slide eight-well high ibiTreat (Ibidi®, Gräfelting, Germany) for direct 24-h fibre treatments. At the end of the experimental time, both cells were fixed with 4% paraformaldehyde (Sigma-Aldrich) in PBS (v/v) for 30 min, permeabilised with 0.1% Triton X-100 (Sigma-Aldrich) in PBS (v/v) for 10 min and incubated with bovine serum albumin (BSA) (Sigma-Aldrich) 3% in 0.1% Triton X-100 for 30 min. Then, they were stained against γ -H2AX (Abcam) as a marker for DNA damage followed by incubation with chicken anti-mouse IgG Antibody, Alexa Fluor™ 488 (Thermo Scientific, USA) and with 2 $\mu\text{g}/\text{ml}$ propidium iodide. Fluorescent signals were captured with Nikon Eclipse AXR confocal microscope equipped with 60 \times NA 1.42 objective for green foci of damaged DNA and red-positive nuclei (excitation at 488 nm for both and emission range of 500–550 nm and 600–670 nm, respectively).

2.12 | Statistical analysis

Data and statistical analyses were performed with GraphPad Prism 8 (GraphPad Software, USA) and are displayed as the mean \pm SD. Statistical significance between the groups was assessed by One-way ANOVA or two-way ANOVA followed by Bonferroni's post-test. A p -value of $p < 0.001$, $p < 0.01$ and $p < 0.05$ was defined as indicating a statistically significant difference.

3 | RESULTS

3.1 | Quantification of fibre metal release

The release of metals from CRO, CHR and ERI (50 $\mu\text{g}/\text{ml}$), which fibrous structure is depicted in Figure 1 by SEM micrographs, was quantified after a 24-h incubation in RPMI medium.

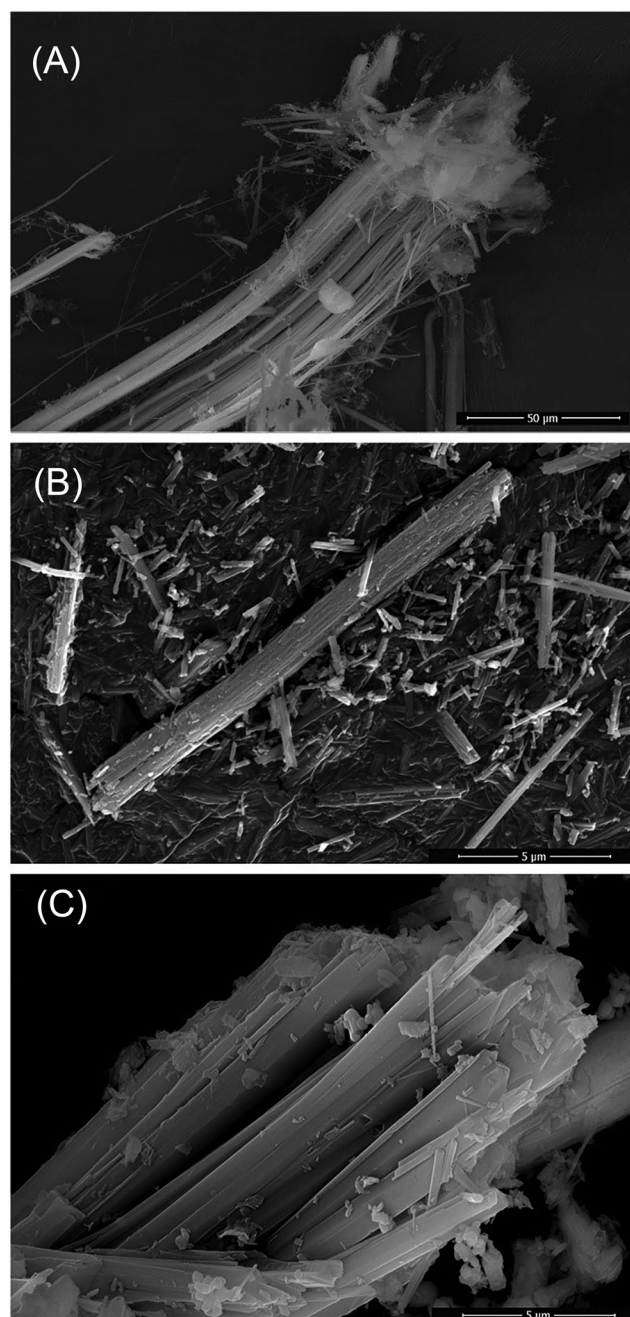


FIGURE 1 High-resolution SEM microphotographs of (A) Balangero chrysotile, CHR, (B) UICC crocidolite, CRO, and (C) Jersey erionite, ERI.

Results reported in Figure 2 showed that CRO did not significantly release any of the investigated metals in the culture medium within the 24-h timeframe. On the contrary, CHR and ERI released significant amounts of metal ions. In detail, CHR released Mg, Cr, Ni and Co, which amounted to a 1.6-, 1.7-, 2.7- and 2.1-fold increase compared to the control medium, respectively. Conversely, ERI released significant amounts of Al (twofold increase) and slight amounts of Mg, as compared to the control medium.

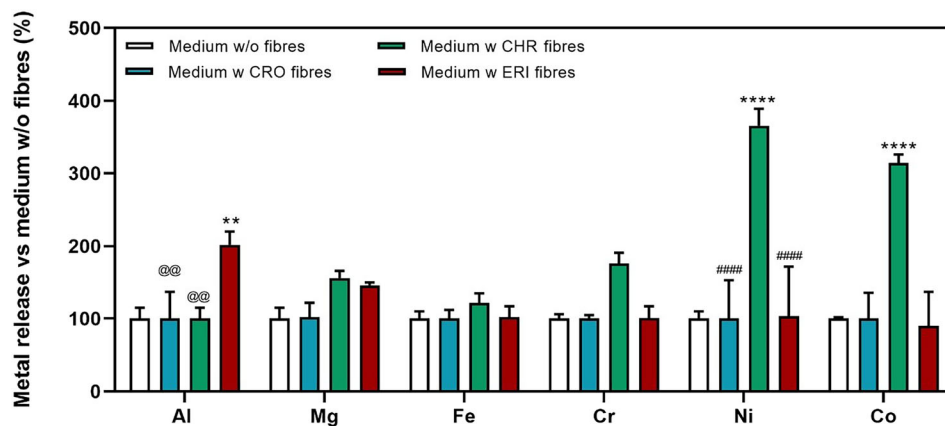


FIGURE 2 Quantification of ion metal release by CRO, CHR and ERI. The release of Al, Mg, Fe, Cr, Ni and Co metal content from the fibres was measured in the RPMI culture medium (pH 7.4) after 24-h incubation at 37°C using inductively coupled plasma–mass spectrometry (ICP-MS). Results are the mean \pm SD of two independent experiments. ** $p < 0.001$, **** $p < 0.0001$ versus medium w/o fibres; @@ $p < 0.01$ versus medium w ERI; #### $p < 0.0001$ versus medium w CHR (two-way ANOVA followed by Bonferroni's post-test).

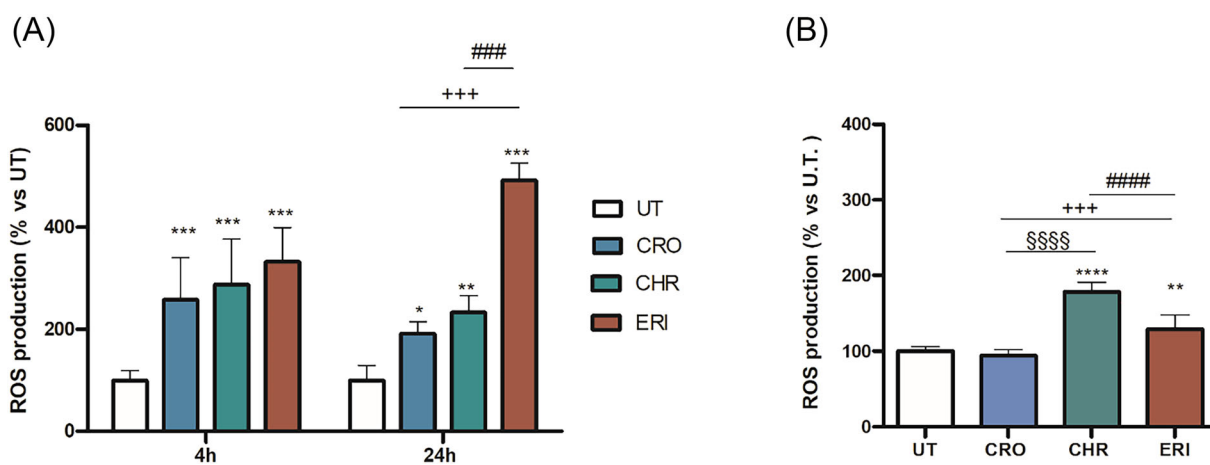


FIGURE 3 Intracellular ROS production in THP-1 and HECV cells. (A) ROS levels in THP-1 cells were analysed by DCF assay after 4 and 24 h of indirect treatment with CRO, CHR and ERI fibres (50 $\mu\text{g}/\text{ml}$). (B) ROS levels in HECV cells after 24 h of direct treatment with fibres (50 $\mu\text{g}/\text{ml}$). Data are expressed as % of ROS production versus untreated (UT) cells (mean \pm SD; $n = 3$). * $p < 0.05$; ** $p < 0.01$; *** $p < 0.001$ versus UT; §§§§ $p < 0.0001$ CRO- versus CHR-; +++ $p < 0.001$ CRO- versus ERI-; #### $p < 0.001$, ##### $p < 0.0001$ CHR- versus ERI-indirectly fibre-treated cells (one-way ANOVA followed by Bonferroni's post-test).

3.2 | Evaluation of ROS levels

The DCF assay quantified the levels of intracellular ROS in THP-1 naïve monocytes and HECV endothelial cells. As shown in Figure 3A, indirect exposure to CRO, CHR, and ERI significantly increased the intracellular ROS levels in THP-1 cells compared to the untreated controls (UT) after 4 and 24 h of incubation. ERI treatment induced the highest time-dependent ROS increase amounting to 3.5- and 4.9-fold increase at 4 and at 24 h, respectively, as compared to UT. Conversely, CRO- and CHR-treated cells showed a higher ROS increase at 4 h compared to 24 h. In HECV cells (Figure 3B), although in direct contact with the fibres, the oxidative stress was comparably lower than that showed in THP-1 monocytes and measurable only at the 24-h treatment. It significantly increased with CHR and ERI

treatments, but not with CRO, compared to UT (1.8- and 1.3-fold increase, respectively).

3.3 | Evaluation of cell toxicity

Initial dose–response experiments were performed on THP-1 cells upon indirect exposure to the fibres and on directly exposed HECV (Figure 4A,B). THP-1 indirect exposure at 24 h (panel A) did not show significant toxicity at any of the concentrations tested for all fibres (from 25 to 100 $\mu\text{g}/\text{ml}$). Conversely, HECV direct exposure (panel B) clearly evidenced a dose–response toxicity with increasing number of dead cells at 24 h with all the fibre tested (from $\sim 25\%$ to $\sim 50\%$ toxicity at 25 and 100 $\mu\text{g}/\text{ml}$, respectively), without significant differences

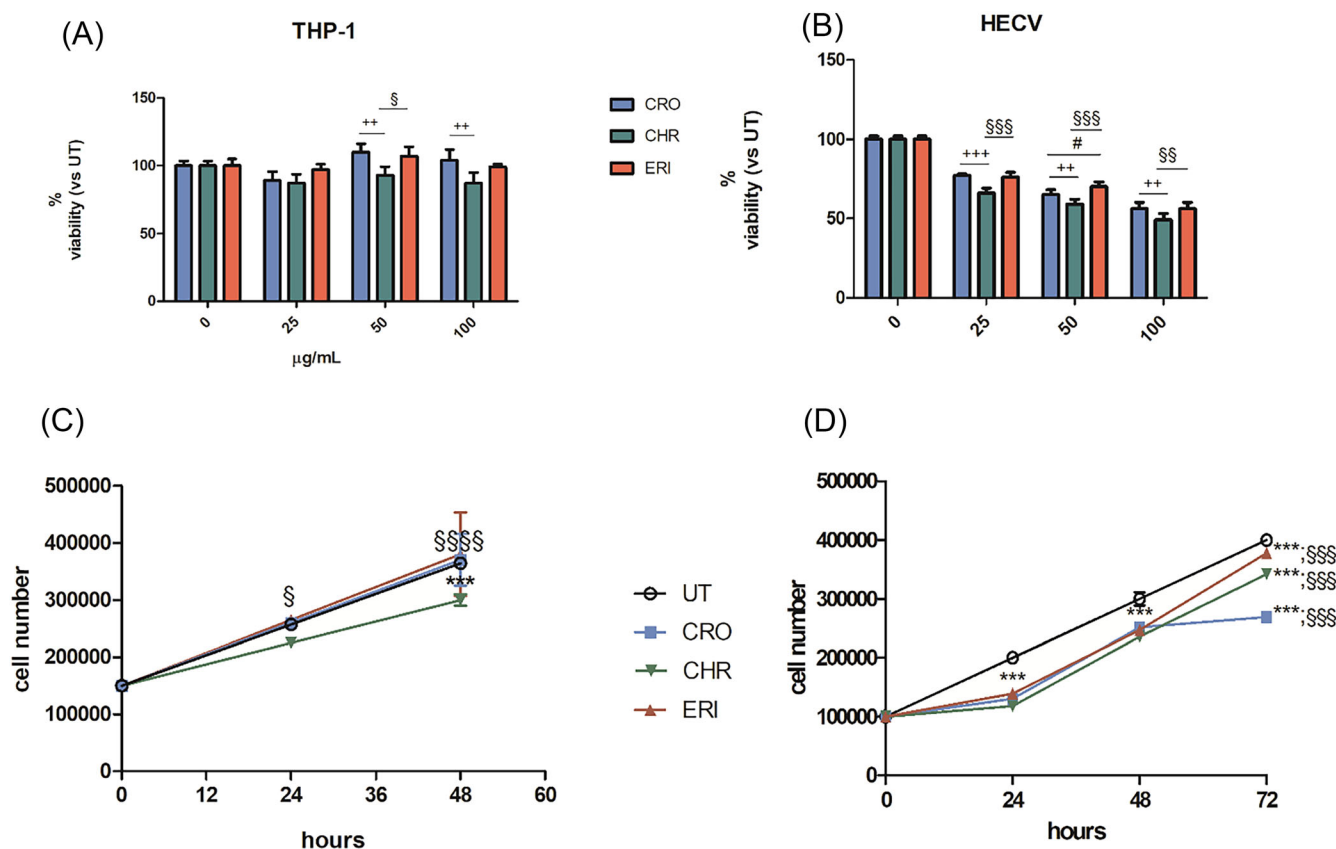


FIGURE 4 Proliferation index of THP-1 monocytes and HECV cells during indirect and direct exposure to fibres. (A,B) Dose–response cell toxicity of THP-1 monocytes (A) and of HECV endothelial cells (B) after 24-h incubation with increasing concentrations of CRO, CHR and ERI mineral fibres (25, 50 and 100 µg/ml, respectively). (C,D) Time course of cell proliferation/toxicity of THP-1 monocytes (C) and of HECV endothelial cells (D) treated with 50 µg/ml CRO, CHR and ERI for the indicated times. THP-1 cells were subjected to indirect treatment while HECV cells to direct treatment, respectively (see Methods for details). Cell proliferation/toxicity was calculated by the Alamar blue DNA quantification assay. * $p < 0.05$, *** $p < 0.001$ versus untreated THP-1 cells; §§ $p < 0.05$ CHR- versus ERI-treated cells, §§§ $p < 0.001$ versus treated cells (two-way ANOVA followed by Bonferroni's post-test).

among the three types of fibres. However, chrysotile showed a slightly higher number of dead cells at the three concentrations tested as compared to the other two fibres.

Thus, the middle concentration (50 µg/ml) was chosen to study more in detail, the toxicity at longer times of exposure, and to study the activation of the following genotoxic/inflammatory pathways, since at this dose there was a certain level of cell damage, especially in HECV, but still a significant number of live cells to be able to assess the intracellular transduction pathways activation and the cellular responses. As shown in Figure 4C, the THP-1 proliferation rate at 48 h was significantly reduced in a time-dependent manner, reaching a 20% reduction only with 50 µg/ml CHR fibre indirect exposure compared to UT, CRO and ERI treated cells. Conversely, HECV proliferation was significantly affected at all time points by the three fibre treatments at the above-mentioned concentration, as depicted in Figure 4D, compared to UT. At 72 h, CRO treatment showed the higher cell viability decrease, reaching a 30% compared to the UT cells. Conversely, at this time point, CHR and ERI treatments showed a milder cell viability impairment, reaching a 15% and 5% cell decrease, respectively, as compared to UT. These data indicate the ability of

HECV to partially overcome the acute toxic effect of the fibres shown at 24 h (panel B) and to restore partially cell proliferation.

3.4 | Evaluation of apoptosis

A quantitative assessment of apoptotic cell death (early and late) affecting THP-1 and HECV cells after 24-h indirect and direct fibre exposure, respectively, was conducted by Annexin V detection and quantification. In general, the rate of apoptosis, independently from the fibre treatments, was significantly higher in THP-1 naïve monocytes as compared to HECV endothelial cells. In detail, for what concerns THP-1, as shown in Figure 5A,B, only CHR significantly induced early and late apoptotic phenomena (27% and 12%, respectively) after indirect treatment at 24 h, compared to UT and to CRO- and ERI-treated cells.

Conversely, in HECV, all three fibre direct treatments determined a significant increase of early and late apoptotic cell death after 24 h, as compared to UT (Figure 5C,D). CRO and CHR had the highest impact in both inducing early and late apoptotic cell death (i.e. 8%–9% for early and 6%–8% for late apoptosis, respectively).

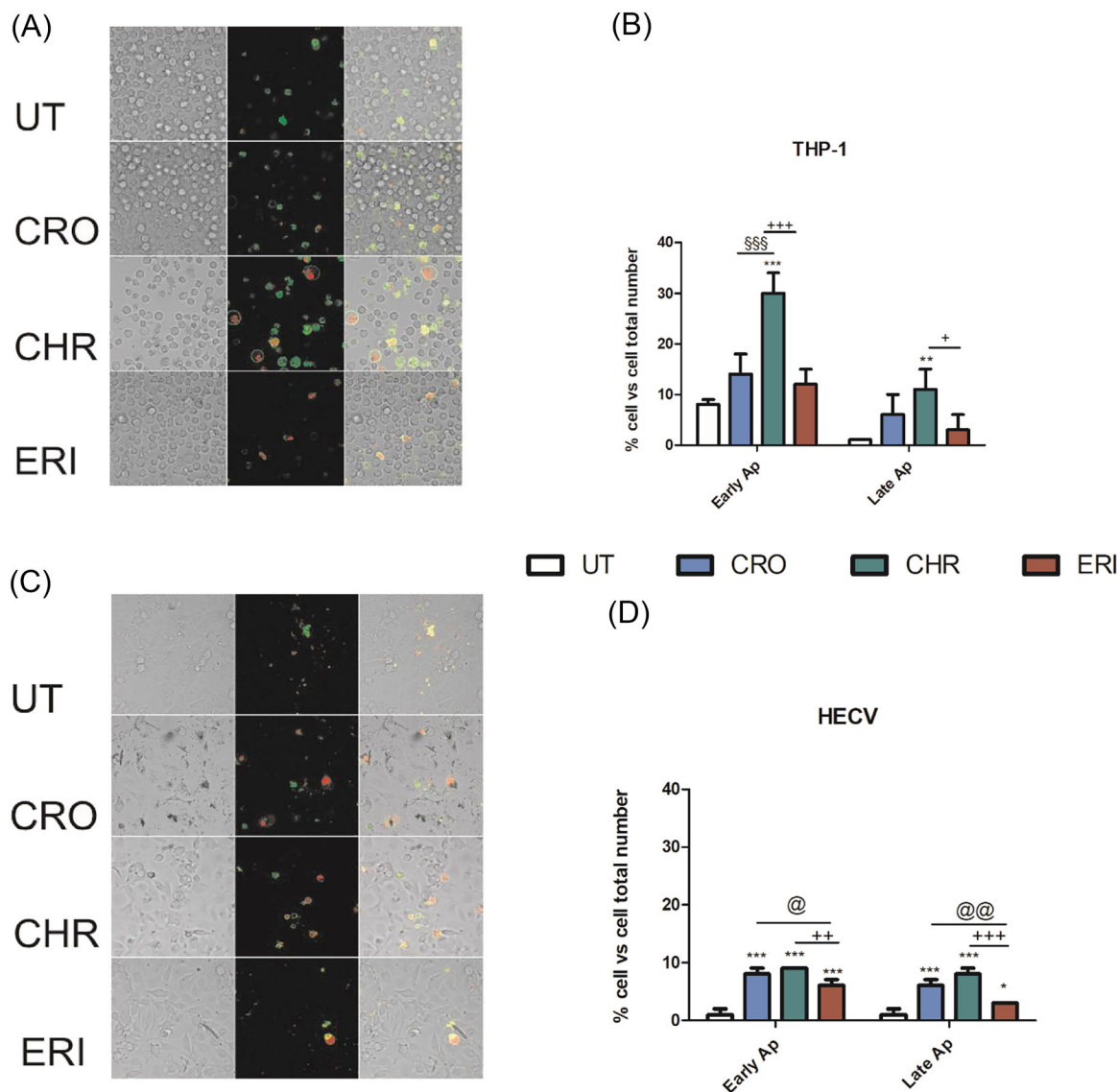


FIGURE 5 Apoptotic cell death analysis by fluorescence microscopy in indirect and direct treated THP-1 and HECV. (A,C) Visualisation by confocal microscopy (2.5× digital zoom) in phase contrast, fluorescence mode and merged images (first, second and third columns, respectively) of (A) THP-1 and (C) HECV cells following 24 h of incubation in the presence or absence of mineral fibres at 50 µg/ml and staining with Annexin V-FITC and propidium iodide. (B,D) The quantitative analysis, inferred from confocal microscopy images, of early (annexin-positive) and late (both annexin- and propidium iodide-positive) apoptotic (B) THP-1 and (d) HECV cells treated with 50 µg/ml of CRO, CHR and ERI relative to the total number of cells counted in light microscopy (results are the mean ± SD of counts from four microphotographs). *** $p < 0.001$, ** $p < 0.01$, * $p < 0.05$ versus untreated cells; §§§ $p < 0.001$ CRO- versus CHR-treated cells; + $p < 0.05$, ++ $p < 0.01$, +++ $p < 0.001$ CHR- versus ERI treated cells; @ $p < 0.05$, @@@ $p < 0.001$ CRO- versus ERI-treated cells (two-way ANOVA followed by Bonferroni's post-test).

3.5 | NF-κB activation and gene expression of pro-inflammatory cytokines and macrophage differentiation markers

The potential pro-inflammatory effect of the indirect treatment of THP-1 monocytes with CRO, CHR and ERI was investigated by analysing the NF-κB signal transduction pathway activation. Subsequently, the expression levels of a panel of dependent genes, namely, IL1-β, TNFα, MCP-1, IL-6 and IL-8 (Figure 6), which are known to be significantly involved in the propagation of the inflammatory signal

both at early and chronic stages (Mantovani et al., 2004), were assessed as well. After 24 h of indirect fibre exposure, a significant NF-κB activation ($p < 0.05$) (Figure 6A,B) and a marked induction of MCP-1, IL-6 and IL-8 gene expression compared to UT (4.8-, 2.7- and 2.3-fold increase, respectively; panel C) were found in CHR-treated THP-1 cells, only. Conversely, CRO and ERI treatments did not show any significant variation of NF-κB activation, while for what concerns the cytokine gene expression, CRO indirect treatment slightly increased the TNFα and IL-1β levels, and ERI promoted IL-8 gene expression and inhibited IL-1β levels.

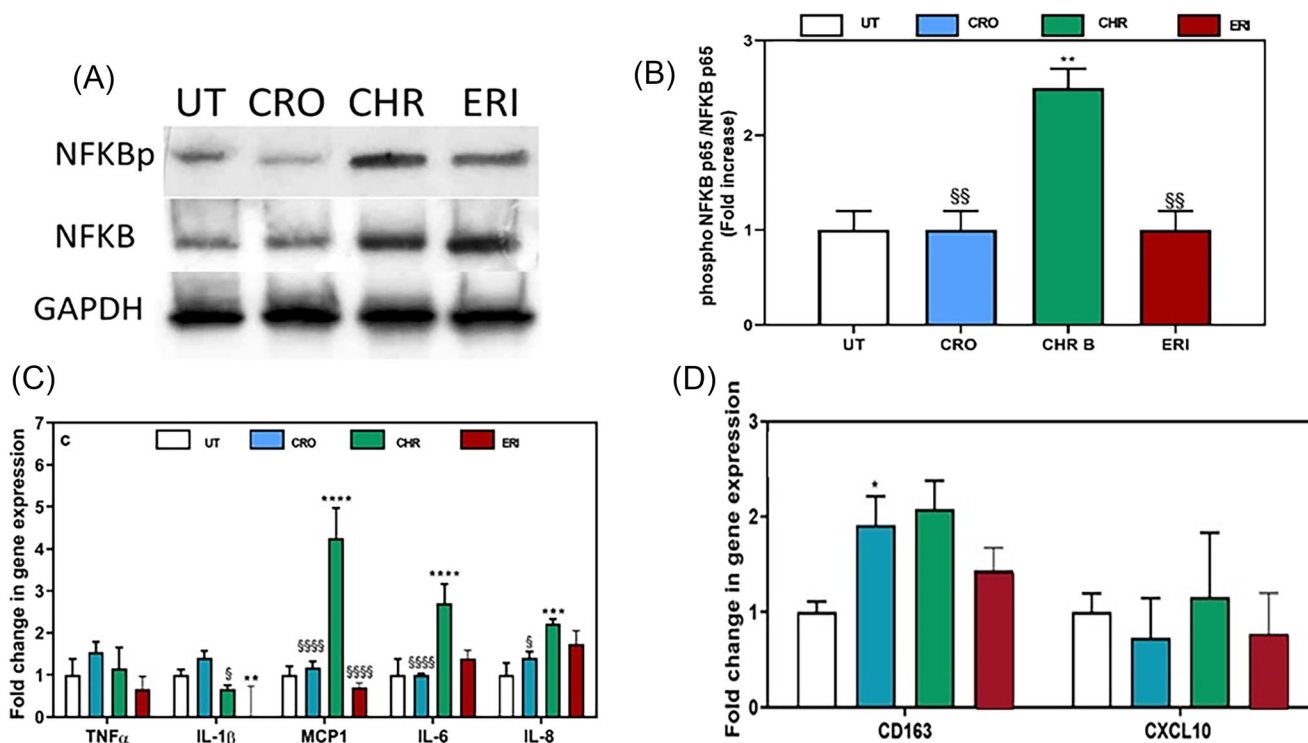


FIGURE 6 NF-κBp65 activation and THP-1 gene expression levels of pro-inflammatory cytokines and macrophage differentiation markers after 24-h indirect fibre exposure. (A) Images are representative of at least three similar immunoblot analyses of NF-κB (p65), phospho-NF-κB (p65) and the housekeeping GAPDH protein level in untreated (UT) and indirectly fibre-treated cells. (B) The bars represent the ratio of phospho-NF-κBp65/NF-κBp65 normalised on the respective GAPDH housekeeping protein and are expressed as fold increase versus untreated THP-1 cells (mean ± SD; $n = 2$). ** $p < 0.01$ versus UT cells; §§ $p < 0.01$ versus indirectly fibre-treated cells (one-way ANOVA followed by Bonferroni's post-test). (C) Gene expression levels of TNF α , IL-1 β , MCP-1, IL-6 and IL-8 pro-inflammatory cytokines in THP-1 monocytes after 24 h of indirect fibre exposure. Data are expressed as fold increase compared to untreated cells (white bars) and are normalised on the expression of the HPRT-1 housekeeping gene (mean ± SD; $n = 3$). **** $p < 0.0001$, *** $p < 0.001$ versus UT cells; §§§§ $p < 0.001$, § $p < 0.05$ versus indirectly fibre-treated cells (two-way ANOVA followed by Bonferroni's test). (D) Gene expression levels of CD163 and CXCL10 macrophage differentiation markers after 24 h of fibre treatments. Data are normalised to the HPRT-1 housekeeping gene and expressed as mRNA-fold increase compared to untreated (UT) THP-1 cells. Results are the mean ± SD of three experiments performed in triplicate. * $p < 0.05$ versus UT (one-way ANOVA followed by Bonferroni's post-test).

The gene expression of the two main M0 macrophage differentiation markers, CD163 and CXCL10, was analysed by qPCR (Figure 6D) in THP-1 monocytes after 24-h indirect treatment. The analysis revealed a twofold increase in the CD163 expression level in CHR- and CRO-treated cells as compared to UT. Conversely, the CXCL10 gene expression profile did not show any significant increase as compared to UT, indicating a tendency, although still at early stages, towards a M0 macrophage phenotype differentiation.

Similar analyses were performed on HECV cells to quantify the pro-inflammatory potential of the fibres during the direct exposure (Figure 7). The NF-κB signal transduction pathway activation (panels A and B) was monitored after 6 h along with the gene expression of a panel of dependent cytokines after 24 h (panel C). Moreover, also VEGF and ICAM-1 gene levels were measured as markers of endothelial inflammatory activation (panel D). Even though the phosphorylated form of NF-κB protein increased only with CRO fibre ($p < 0.01$, panels A and B), all three fibres induced a significant gene expression increase of IL-1 β (over 1.9-folds) and IL-6 cytokines (1.47-, 1.95- and 1.53-fold for CRO, CHR and ERI, respectively,

panel C). In particular, CRO and ERI also increased IL-8 mRNA expression after 24 h (1.45- and 1.56-fold, respectively). For what concerns the endothelial markers VEGF and ICAM-1 after exposure to the three fibres for 24 h, the qPCR analysis showed no significant changes for the growth factor VEGF expression as compared to UT and conversely a similar increase for the intercellular adhesion molecule ICAM-1, which increases vascular permeability and mediates interactions with immune cells (about 1.5-fold compared with untreated cells).

A further investigation was performed to measure the release of IL-1 β and TNF- α proteins in THP-1 and HECV cell media by ELISA quantification after 24-h fibre treatment (Figure 8). In THP-1, only CHR indirect treatment induced a significant increase in the IL-1 β cytokine release at 24 h compared to UT (57 vs. 37 $\mu\text{g/ml}$, respectively, panel A), and its inhibition by the ERI fibre treatment was confirmed (17 $\mu\text{g/ml}$), in agreement with the gene evaluation profile. Also, the TNF- α release quantification confirmed the gene expression analysis of the same cytokine at 24 h, with no differences observable in all fibre treatments as compared to UT.

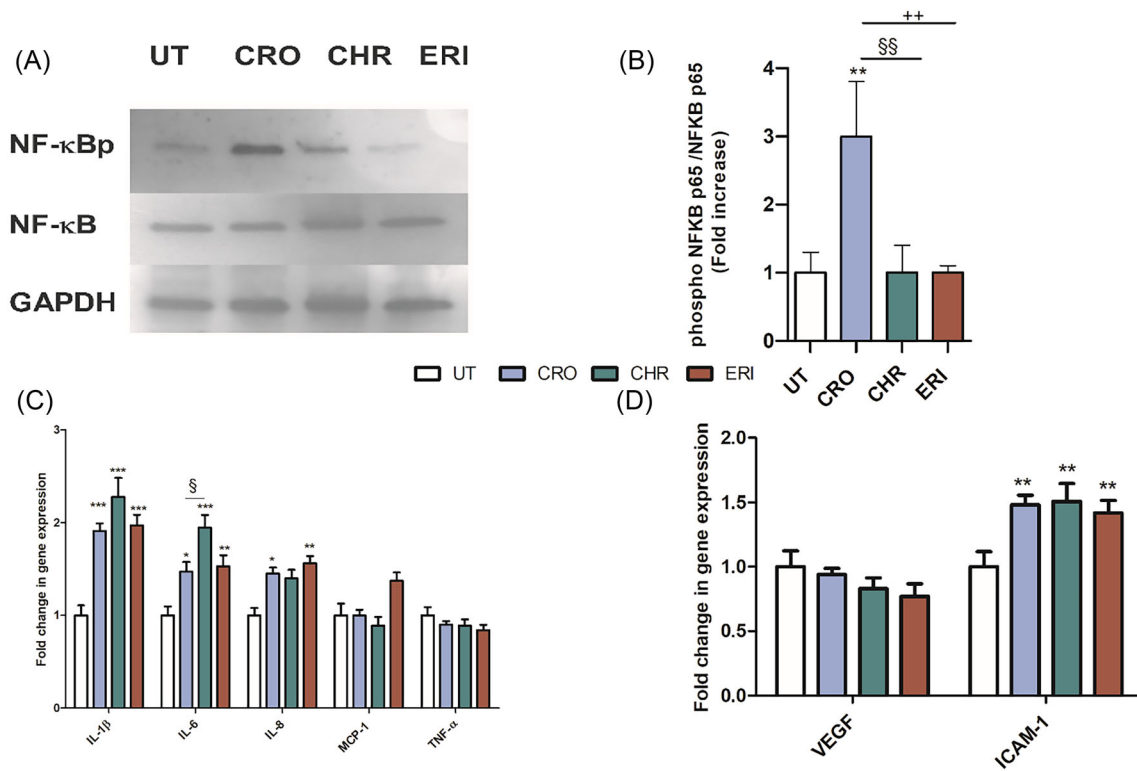


FIGURE 7 NF-κBp65 activation and gene expression levels of HECV cell inflammation markers after 24-h direct fibre exposure. (A) Images are representative of at least three similar immunoblot analyses of NF-κB (p65), phospho-NF-κB (p65) and the housekeeping GAPDH protein level in untreated (UT) and directly fibre-treated cells. (B) The bars represent the ratio of phosphoNF-κBp65/NF-κBp65 normalised on the respective GAPDH housekeeping protein and are expressed as a fold increase versus untreated HECV cells (mean ± SD; n = 2). **p < 0.01 versus UT cells; §§p < 0.01 versus directly CRO and CHR fibre-treated cells; ++p < 0.01 CRO- versus ERI-treated cells (one-way ANOVA followed by Bonferroni's post-test). (C) Gene expression levels of TNFα, IL-1β, MCP-1, IL-6 and IL-8 cytokines and (D) VEGF and ICAM-1 endothelial activation markers in HECV cells after 24 h of direct fibre exposure. Data are expressed as fold increase compared to untreated cells (white bars) and are normalised on the expression of the GAPDH housekeeping gene (mean ± SD; n = 3). ****p < 0.0001, ***p < 0.001 versus UT cells; §§p < 0.01, §p < 0.05 CRO- versus CHR-, ++p < 0.01 CRO versus ERI- directly fibre-treated cells (two-way ANOVA followed by Bonferroni's test).

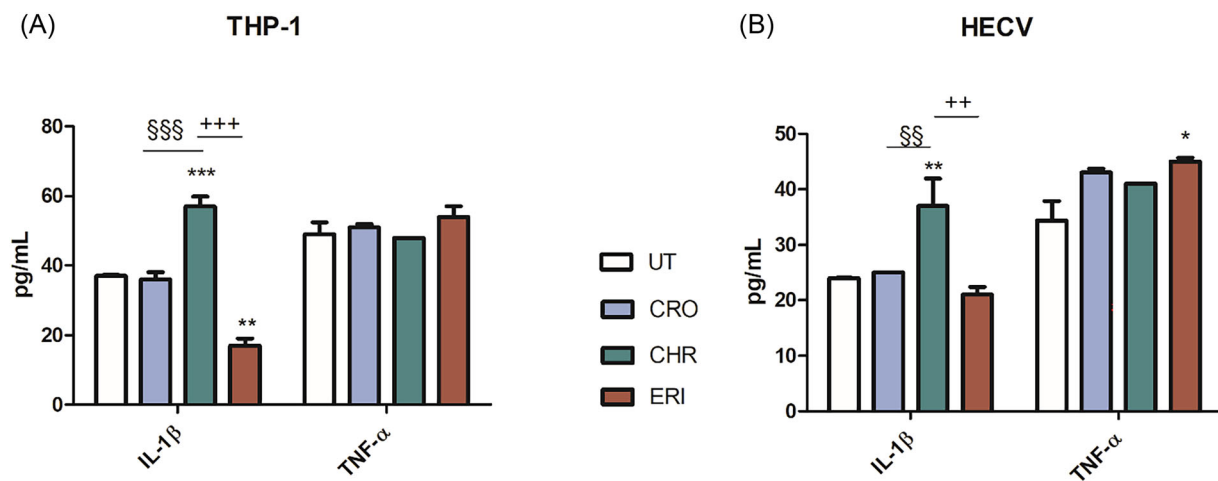


FIGURE 8 IL-1β and TNF-α proteins released into the extracellular medium of (A) THP-1 and (B) HECV cells exposed to fibres. ELISA assay was performed after 24 h of fibre treatment (50 µg/ml) quantifying IL-1β and TNF-α cytokine content (µg/mL) in the extracellular medium. Results are the mean ± SD of two experiments performed in triplicate. *p < 0.05, **p < 0.01, ***p < 0.001 versus UT; §§§p < 0.001, §§p < 0.01 CRO versus CHR treated cells; +++p < 0.001, ++p < 0.01 CHR versus ERI treated cells (two-way ANOVA followed by Bonferroni's post-test).

The parallel measurement of IL-1 β and TNF- α cytokines released by HECV in the extracellular media (panel B) revealed a significant increase of IL-1 β only in CHR fibre treatment as compared to UT (37 vs. 24 $\mu\text{g}/\text{ml}$, respectively). Conversely, a TNF- α increased extracellular release was detected only in ERI-treated cell media as compared to UT (45 vs. 34 $\mu\text{g}/\text{ml}$, respectively).

3.6 | Analysis of the genotoxic effects

To investigate whether the indirect and direct exposure to the three mineral fibres could exert genotoxic effects on THP-1 and HECV cells, the rate of DNA double-strand breaks (DBS), in terms of γ -H2AX protein levels, was quantified after 24-h treatments by both immunoblot and confocal microscopy analyses (Figures 9 and 10). As shown in Figure 9, the γ -H2AX protein levels were significantly increased ($p < 0.0001$) in all fibre-exposed THP-1 compared to UT. Notably, CRO, CHR and ERI increased to 37-, 72- and 47-fold the γ -H2AX/H2AX ratio analysed by immunoblot (panels A and B). Consistently, these data were confirmed by confocal microscopy images (panel C),

where the number of γ -H2AX foci (in green) was significantly increased in the nuclei (in red) of fibre-exposed THP-1 cells compared to UT. On the contrary, in fibre-treated HECV (Figure 10), there was a significant increase in phosphorylated H2AX protein only after exposure to CRO and CHR fibres with expression levels, analysed by immunoblot, approximately twofold higher than in UT (panels A and B). The western blot analysis was further validated by confocal imaging (panel C) highlighting an increased number of fluorescent green γ -H2AX foci in CRO- and CHR-treated HECV as compared to the other experimental conditions (i.e. UT and ERI-treated).

4 | DISCUSSION

Still nowadays, respirable mineral fibres like chrysotile, amphibole asbestos and fibrous erionite (shown in Figure 1) are recognised as a serious risk factor to human health because exposure to these airborne carcinogens may occur in both working and natural (non-working) environments. Inhalable fibres are the total airborne fibres that are inhaled through the nose and mouth. Respirable fibres are the

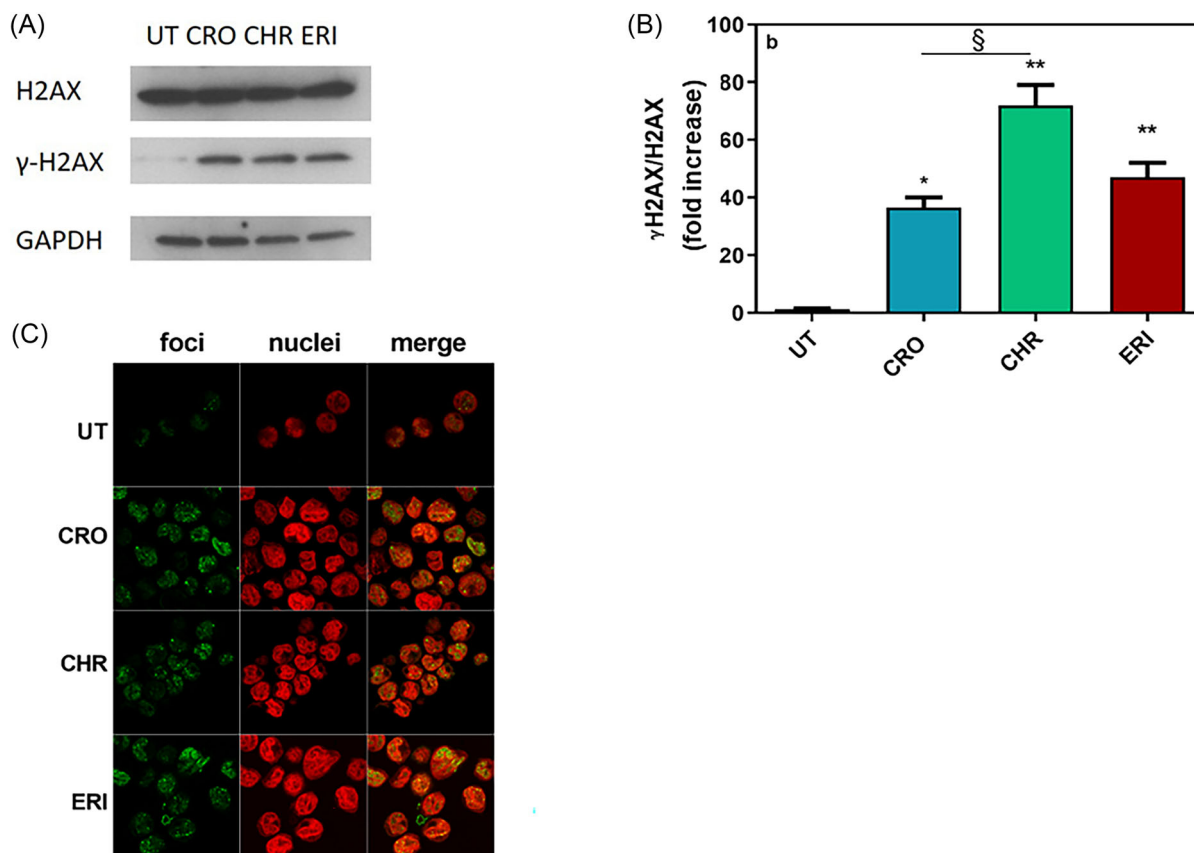


FIGURE 9 Evaluation of fibre-induced genotoxic damage in THP-1 monocytes at 24 h. (A) Representative image of at least three similar immunoblot analyses of H2AX, γ -H2AX (phospho-Ser139) and housekeeping GAPDH protein levels in untreated and fibre-treated THP-1. (B) The bars show the ratio of γ H2AX/H2AX protein expression from immunoblot images, normalised on the GAPDH housekeeping protein in untreated (UT) and indirect fibre-treated cells and is expressed as fold increase versus UT (mean \pm SD; $n = 3$) * $p < 0.05$, ** $p < 0.01$ versus untreated cells; $\S p < 0.05$ CRO- versus CHR-treated cells (one-way ANOVA followed by Bonferroni's post-test). (C) Confocal microscopy analysis of γ H2AX protein as a marker of DNA double-strand breaks foci (green staining), in the cell nuclei (propidium iodide, red staining) of untreated and fibre-treated THP-1 monocytes.

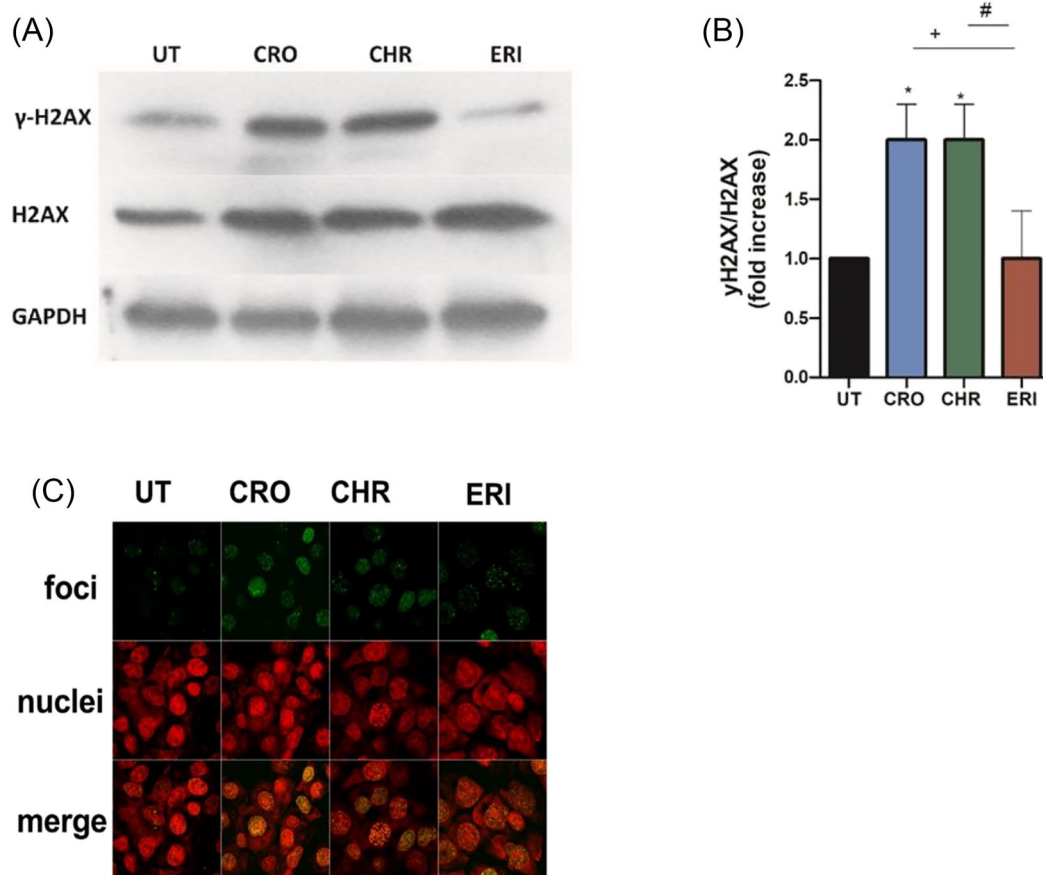


FIGURE 10 Evaluation of fibre-induced genotoxic damage in HECV cells at 24 h. (A) Representative image of at least three similar immunoblot analyses of H2AX, γ -H2AX (phospho-Ser139) and housekeeping GAPDH protein levels in untreated and fibre-treated HECV. (B) he bars show the ratio of γ H2AX/H2AX protein expression from immunoblot images, normalised on the GAPDH housekeeping protein in untreated (UT) and fibre-treated cells and is expressed as fold increase versus UT (mean \pm SD; $n = 3$) * $p < 0.05$, ** $p < 0.01$ versus untreated cells; + $p < 0.05$ CRO- versus ERI-treated cells; # $p < 0.05$ CHR- versus ERI-treated cells (one-way ANOVA followed by Bonferroni's post-test). (C) Confocal microscopy analysis of γ -H2AX protein as a marker of DNA double-strand breaks (green staining) in the cell nuclei (propidium iodide, red staining) of untreated and fibre-treated HECV cells.

fraction of inhaled fibres penetrating the unciliated airways and reaching the deep respiratory system (lung alveoli). According to the WHO definition, respirable fibres are those with length $L > 5 \mu\text{m}$, width $W < 3 \mu\text{m}$ and L/W ratio (aspect ratio) $> 3:1$.

As far as the working environment is concerned, despite the claim of some countries of being able to 'safely' mine, manufacture and use chrysotile, the risk of exposure in following operations like maintenance of contaminated materials, demolition and disposal is still very much an issue (Borges et al., 2022; Gualtieri, 2021; WHO, 2014). As known, the inhalation of asbestos fibres is considered a key event in the onset of several pulmonary diseases. Several features of asbestos and zeolite fibres, including their chemical composition and bio-persistence, as well as their structure, net charge, zeta potential, interacting capability and so on, are involved in their toxic and carcinogenic effects (Giordani et al., 2022). As reported in Gualtieri (2021), there are several parameters of mineral fibres involved in prompting adverse effects responsible for immunotoxic patho-biological processes (IARC nr. 7 'immunosuppression' Key carcinogenicity

parameter). Specifically, for immunosuppression these fibres' parameters are length, hydrophilicity/hydrophobicity, surface area, content of iron and metals, dissolution rate and related release of iron and metals, zeta potential (surface charge) and fibres' aggregation. Hence, the different nature of chrysotile, crocidolite and erionite in terms of fibre parameters reflects in different immunotoxic responses (Gualtieri, 2021, 2023). For chrysotile, the major parameters playing a role are the large surface area and its hydrophilic character, the fast dissolution rate (non-biodurability) with release of iron and metals and the fibres' aggregation due to the surface charge. For crocidolite, the major parameters playing a role are the fibre length, hydrophilicity of the surface and content of iron and metals chronically active at the (biodurable) surface of the fibres. For erionite, they are the hydrophilicity of the surface, the content and release of alkaline ions and the fibres' aggregation due to the surface charge.

The literature reports two main different molecular mechanisms to describe the involvement of asbestos minerals in cancer development: one regarding their direct effect on DNA damage by mechanical

interference with chromosomal segregation during cellular mitosis and the other related to their ability to induce the production of mutagenic ROS and inducible NO synthase in mesothelial cells and macrophages (Carbone & Yang, 2012).

Despite the large amount of literature on the subject, information is still lacking on some of the molecular mechanisms involved in the toxicity and inflammatory potential of asbestiform fibres, ultimately leading to lung fibrosis and tumour development. An overlooked subject is the contribution given by the release of heavy metals, ions and other contaminants leaking from the fibres in the extracellular environment. Indeed, these factors can exert cytotoxic and pro-inflammatory effects by themselves aggravating the cellular damage already produced by the mechanical contact with the fibres and activating cellular responses favouring cell transformation.

Thus, to investigate the contribution of soluble factors released by the mineral fibres, in this study, we evaluated the indirect effects of CRO, CHR and ERI in human THP-1 monocytes physically separated from the fibres by the presence of a semipermeable membrane. The analyses of pro-inflammatory and genotoxic processes as possible early fibre-related toxicity indicators were performed to better understand the influence of fibre-released soluble factors. Moreover, by comparison, we also report the direct fibre effects on human HECV endothelial vein cells as part of the lung structure involved in the damage response. Indeed, it has been reported the contribution of these cells to the development of different acute and chronic inflammatory pulmonary disorders (Treadwell et al., 1996), although still not accurately investigated with the above-mentioned mineral fibres.

Given that trace metals in fibres play a crucial role in ROS production and cancer development, we quantified the release of several heavy metals (i.e. Al, Mg, Fe, Cr, Ni and Co) known to be present in the investigated mineral fibres (Bloise et al., 2016) into the cell culture medium at pH 7.4 simulating the extracellular fluids (Figure 2). As expected, in 24 h, CHR released the highest amounts and variety of trace metals as compared to the other minerals, according to its low biodurability. These metals, in particular Ni and Co (Chen et al., 2003; Kawanishi et al., 2001; Nackerdien et al., 1991; Salnikow et al., 2000), are known to be hazardous to human health due to their ability to generate ROS. Conversely, the medium with ERI resulted enriched in Al ions, released from the fibre surface by a dealumination process. This release can increase the oxidative stress in THP-1 after the ERI treatment. In fact, Al is able to free iron from Fe-containing enzymes and proteins leading to the generation of ROS (Han et al., 2013). On the other side, also the ability of ERI fibres to exchange cations like K^+ , Ca^{++} and Na^+ within the extracellular/intracellular environment could contribute to the overall damage by dysregulating the Ca^{++} crosstalk and the Na^+/K^+ cellular homeostasis, resulting in an increased cellular oxidative stress (Gualtieri, 2023).

In this study, the different cellular response intensities are related both to the nature of the two cell lines and to the different way of exposure to the fibres. Regarding the different cell types, while both showing an increase in the oxidative stress (Figure 3) and in the apoptosis rate (Figure 5) in all treatments with fibres as

compared to untreated cells, these parameters were significantly lower in directly exposed HECV endotheliocytes than in indirectly exposed THP-1 monocytes. This is quite surprising because the monocytes are not in direct contact with the fibres, yet they result the most sensitive. It likely occurs because they are immune cells able to differentiate to active phagocytes in the presence of potentially harmful substances, such as metal ions. Therefore, monocytes are much more sensitive to external triggers promoting their activation and differentiation towards a macrophage inflammatory phenotype (Bassi et al., 2023). Starting with these observations, we then acknowledged other differences in the biological responses of the two cell lines, this time more related to type of exposure to the fibres. The evaluation of THP-1 biological responses clearly showed that indirect exposure to CHR fibres was able to induce the most significant effects in terms of toxicity (Figure 4A), apoptosis (Figure 5A,B), NF- κ B activation, inflammatory cytokine production, macrophage differentiation (Figure 6 and 8A) and genotoxic damage (Figure 9). Thus, the CHR-released metal ions likely act as soluble mediators of toxicity and inflammation leading to the clear biological effects observed in monocytes.

On the other hand, the HECV responses seem more related to the direct contact with the mineral fibres, all three types mainly exerting their damaging potential at the level of the cell surface, since endothelial cells are not phagocytes, and in fact, they show effects comparable to those of A549 alveolar cells, investigated in a previous study with the same fibres (Bassi et al., 2023). Thus, despite the type of fibre, HECV show similar levels of responses as compared to untreated cells in terms of toxicity (Figure 4B), apoptosis percentage (Figure 5C,D), pro-inflammatory cytokine production (Figure 8B), endothelial activation markers (Figure 7D) and genotoxic damage (Figure 10). The only exceptions are the NF- κ B activation and the ROS production. Although only CRO promotes the phosphorylation of NF- κ B protein after 6-h exposure (Figure 7A,B), justifying the following pro-inflammatory cytokine and endothelial marker production by this fibre, for the CHR- and ERI-treated HECV, very likely it is the intracellular ROS production the key pathway through which the pro-inflammatory reaction is triggered with these types of fibres. In any way, the two pathways seem to lead to the same downstream effects. Another relevant effect in HECV is the gene overexpression of ICAM-1 with all three fibres, which can cause increase of vascular permeability, enhanced chemoattracted immune cell extravasation and the loss of the endothelial barrier function with related cytoskeletal reorganisation leading to chronic effects on the lung tissue function, such as the onset of fibrosis (Clark et al., 2007).

Overall, these observations highlight the diverse biological responses to the mineral fibres related to their different content of exchangeable metal ions and their physicochemical properties also affecting their biodurability (Camus, 2001; Gualtieri et al., 2019; McDonald & McDonald, 1997). They establish how CHR, being a non-biodurable fibre (Gualtieri, 2023; Gualtieri et al., 2018; Li et al., 2012), releases significant amounts of redox-active metals in amounts sufficient to induce activation of monocyte cells circulating in the alveolar capillaries. We are not able to give a clear answer to the question if

the same cascades of pathways are activated by CHR treatment of THP-1 and HECV cells, although the downstream responses are similar in the two cell types. Some mechanisms could be the same, such as the ROS increase, which is observed in both cells, while other could be different like the NF- κ B activation pathway, which is observed only in THP-1 cells and not in HECV. It is also important to highlight that the two cell types are not treated in the same way, since monocytes are not in direct contact with the fibres as the endothelial cells are. Thus, in the first case we only see the effects of the soluble metal ions and other impurities reaching the cells, while in the second there is mainly the contribute of direct cell contact of the fibres with the cell membranes. Consequently, it is not surprising if the downstream responses of the two types of cells, although ultimately the same, are triggered by different transduction pathways.

The effects of CRO seem to be elicited mainly because of cellular direct contact with its iron-rich surface promoting the intracellular oxidative stress (Gualtieri, 2021). Thus, we can assume that the early increase in ROS production found in CRO indirectly treated THP-1 cells may be due to the release of other soluble toxic factors that we did not identify in this study, surely deserving further investigation.

Concerning the acute ERI effects, these are milder in the two cell types, both indirectly and directly exposed, as compared to CRO and CHR, as highlighted in the summary of Table 3. In Di Giuseppe et al. (2022), our group reported that erionite, differently from other mineral fibres such as CRO and CHR, is not able to elicit a substantial intracellular Ca^{2+} increase after cell treatment. Thus, our hypothesis is that, despite the significant ROS production observed in THP-1 cells, erionite is not able to cause an early significant inflammatory response because somehow the Ca^{2+} signalling, essential for the activation of the main intracellular inflammatory pathways, is impaired by some chemical property specific of erionite as compared to the other mineral fibres. Indeed, the explanation of the biochemical mechanisms leading to the reduced intracellular Ca^{2+} signalling, and the imbalance

of other important cations in THP-1 cells upon erionite treatment, is a topic that our group is meant to address in future studies, since it could be of master importance for the global understanding of erionite mechanisms of toxicity and carcinogenicity.

In broad terms, these data from the current study confirm our previously reported data on a similar intracellular metal ion release in THP-1-derived MO macrophages after phagocytosis of the same three types of fibres (Thyssen et al., 2018). The only exception is the significant intracellular Fe leakage from CRO and CHR observed after their phagocytosis, which is not reflected by incubation in the extracellular medium and is probably due to the lower pH of the macrophage phagolysosome. Thus, even though the intracellular environment exacerbates the leakage of metals from the mineral fibres, a significant and potentially toxic release of ions seems to already occur in the early moments of respiration when the fibres encounter the extracellular body fluids, such as saliva, mucus and alveolar surfactant, likely promoting early inflammatory responses. On the other hand, also endothelial cells, upholstering the lung capillaries just below the thin alveolar cell layer, seem to take part to these early pro-inflammatory responses when coming to contact with the fibres due to their penetration in the alveolus wall.

Thus, we can conclude that, although ERI in vivo studies showed higher carcinogenicity than CHR and CRO (Gualtieri et al., 2016), in this study, all three fibres activated early cellular response mechanisms, which if persistent, in the case of mineral fibres from months to years, can lead to a chronic inflammatory condition and the development of chronic diseases (i.e. fibrosis, lung cancer and MM) characterised by long latency periods and late diagnosis (Cox, 2019).

Therefore, the circulating THP-1 monocytes and adherent HECV endothelial cells can be considered valid and effective models for evaluating the early cytotoxic and genotoxic potential of mineral fibres that, despite their biodurability, are able to release both trace elements and soluble impurities into the cellular medium, actively contributing to the following detrimental effects.

TABLE 3 Summary of the chemical-biological effects of the three mineral fibres.

	Crocidolite CRO		Chrysotile CHR		Erionite ERI	
	THP-1	HECV	THP-1	HECV	THP-1	HECV
Metal ion release in the extracellular medium	—		Mg, Ni, Cr, Co		Al, Mg	
Cell type	THP-1		THP-1		THP-1	
• THP-1 indirect exp.	—		—		—	
• HECV direct exp.	—		—		—	
Cytotoxicity	—	**	*	*	—	*
Apoptosis	—	*	**	*	—	*
ROS production	**	-	**	**	***	*
NF- κ B activation	—	*	*	—	—	—
DNA damage	**	*	***	*	**	—
Cytokine release	—	—	*	*	—	—
Inflammatory gene upregulation	—	**	**	**	—	**

Notes: The number of asterisks indicates the degree of the observed effects in the experiments performed in this study. In THP-1 cells, the effects derive from indirect exposure by physical separation through a semipermeable membrane; conversely, in HECV cells, the responses come from direct exposure to the fibres.

5 | CONCLUSIONS

In summary, as shown in Table 3, the early effects of the three carcinogenic fibres (i.e. crocidolite UICC, Balangero chrysotile and fibrous erionite from Jersey) were observed in two different in vitro cell models consisting of THP-1-naïve monocytes cultured in an insert-equipped plate and indirectly treated with the fibre suspensions and HECV endothelial cells directly treated in monolayer cultures.

Although chrysotile has so far been considered the least dangerous among these fibres because of its low biodurability, in this study, it was seen to trigger early immune responses in THP-1-naïve cells by decreasing cell proliferation and activating inflammatory mechanisms, unlike CRO and ERI, which, despite both having been classified as more toxic than chrysotile, due to their physical and chemical characteristics, were not shown to equally activate the immune response in the early stages of fibre inhalation. Conversely, this difference of toxicity is not evinced in the HECV endothelial model in which the fibres enter in direct contact with the cells and the observed effects seem more related to the structural and physical characteristics of the fibres, rather than the release of soluble factors into the extracellular medium.

In conclusion, our study provides clarification on some aspects of the first inflammatory and cytotoxic stages of long latency-pulmonary diseases (i.e. asbestosis, MM and lung carcinoma) following the inhalation of mineral fibres and their deposition in the lung environment. Moreover, these results provide new findings to the complex and controversial scenario of mineral fibre toxicity.

CONFLICT OF INTEREST STATEMENT

The authors declare no conflicts of interest.

DATA AVAILABILITY STATEMENT

All raw data will be available upon request.

ORCID

Serena Mirata  <https://orcid.org/0000-0003-3395-9579>

Sonia Scarfi  <https://orcid.org/0000-0002-7079-6919>

REFERENCES

- Aarskog, N., & Vedeler, C. (2000). Real-time quantitative polymerase chain reaction. *Human Genetics*, 107, 494–498. <https://doi.org/10.1007/s004390000399>
- Ballirano, P., Bloise, A., Gualtieri, A. F., Lezzerini, M., Pacella, A., Perchiizzi, N., Dogan, M., & Dogan, A. U. (2017). The crystal structure of mineral fibres. In A. F. Gualtieri (Ed.), *Mineral fibres: Crystal chemistry, chemical-physical properties, biological interaction and toxicity* (pp. 17–64). Mineralogical Society of Great Britain & Ireland. <https://doi.org/10.1180/EMU-notes.18.2>
- Bassi, A. M., Mirata, S., Almonti, V., Tirendi, S., Vernazza, S., Fornasini, L., Raneri, S., Bersani, D., Passalacqua, M., Gualtieri, A. F., & Scarfi, S. (2023). Cytotoxic and pro-inflammatory early effects of mineral fibres on human alveolar epithelial and immune cells. *Periodico di Mineralogia*, 92, 223–239. <https://doi.org/10.13133/2239-1002/18082>
- Baur, X., & Frank, A. L. (2021). Ongoing downplaying of the carcinogenicity of chrysotile asbestos by vested interests. *Journal of Occupational Medicine and Toxicology*, 16, 6. <https://doi.org/10.1186/s12995-021-00295-2>
- Bernstein, D. M., Toth, B., Rogers, R. A., Kunzendorf, P., Phillips, J. I., & Schaudien, D. (2021). Final results from a 90-day quantitative inhalation toxicology study evaluating the dose-response and fate in the lung and pleura of chrysotile-containing brake dust compared to TiO₂, chrysotile, crocidolite or amosite asbestos: Histopathological examination, confocal microscopy and collagen quantification of the lung and pleural cavity. *Toxicology and Applied Pharmacology*, 424, 115598. <https://doi.org/10.1016/j.taap.2021.115598>
- Bloise, A., Barca, D., Gualtieri, A. F., Pollastri, S., & Belluso, E. (2016). Trace elements in hazardous mineral fibres. *Environmental Pollution*, 216, 314–323. <https://doi.org/10.1016/j.envpol.2016.06.007>
- Borges, R., Giroto, A. S., Guimarães, G. G. F., Reis, H. P. G., Farinas, C. S., & Ribeiro, C. (2022). Asbestos cement waste treatment through mechanochemical process with KH₂PO₄ for its utilization in soil pH correction and nutrient delivery. *Environmental Science and Pollution Research*, 29, 28804–28815. <https://doi.org/10.1007/s11356-021-17679-w>
- Bosshart, H., & Heinzelmann, M. (2016). THP-1 cells as a model for human monocytes. *Annals of Translational Medicine*, 4(21), 4–7. <https://doi.org/10.21037/atm.2016.08.53>
- Broadus, V. C., Yang, L., Scavo, L. M., Ernst, J. D., & Boylan, A. M. (1997). Crocidolite asbestos induces apoptosis of pleural mesothelial cells: Role of reactive oxygen species and poly (ADP-ribosyl) polymerase. *Environmental Health Perspectives*, 105, 1147–1152. <https://doi.org/10.1289/ehp.97105s51147>
- Camus, M. (2001). A ban on asbestos must be based on a comparative risk assessment. *Canadian Medical Association Journal*, 164, 491–494.
- Carbone, M., Baris, Y. I., Bertino, P., Brass, B., Comertpay, S., Dogan, A. U., Gaudino, G., Jube, S., Kanodia, S., Partridge, C. R., Pass, H. I., Rivera, Z. S., Steele, I., Tuncer, M., Way, S., Yang, H., & Miller, A. (2011). Erionite exposure in North Dakota and Turkish villages with mesothelioma. *Proceedings of the National Academy of Sciences U.S.A.*, 108, 13618–13623. <https://doi.org/10.1073/pnas.1105887108>
- Carbone, M., & Yang, H. (2012). Molecular pathways: Targeting mechanisms of asbestos and erionite carcinogenesis in mesothelioma. *Clinical Cancer Research*, 18, 598–604. <https://doi.org/10.1158/1078-0432.CCR-11-2259>
- Chen, L., Yang, X., Jiao, H., & Zhao, B. (2003). Tea catechins protect against Lead-induced ROS formation, mitochondrial dysfunction, and calcium dysregulation in PC12 cells. *Chemical Research in Toxicology*, 16, 1155–1161. <https://doi.org/10.1021/tx0340605>
- Clark, P. R., Manes, T. D., Pober, J. S., & Kluger, M. S. (2007). Increased ICAM-1 expression causes endothelial cell leakiness, cytoskeletal reorganization and junctional alterations. *Journal of Investigative Dermatology*, 127(4), 762–774. <https://doi.org/10.1038/sj.jid.5700670> Epub 2006 Dec 28. PMID: 17195014
- Cox, L. A. Jr. (2019). Dose-response modeling of NLRP3 inflammasome-mediated diseases: Asbestos, lung cancer, and malignant mesothelioma as examples. *Critical Reviews in Toxicology*, 49, 614–635. <https://doi.org/10.1080/10408444.2019.1692779>
- Dalsgaard, S. B., Würtz, E. T., Hansen, J., Røe, O. D., & Omland, Ø. (2021). Cancer incidence and risk of multiple cancers after environmental asbestos exposure in childhood—A long-term register-based cohort study. *International Journal of Environmental Research and Public Health*, 19, 268. <https://doi.org/10.3390/ijerph19010268>
- Di Giuseppe, D., Scarfi, S., Alessandrini, A., Bassi, A. M., Mirata, S., Almonti, V., Ragazzini, G., Mescola, A., Filaferrò, M., Avallone, R., Vitale, G., Scognamiglio, V., & Gualtieri, A. F. (2022). Acute cytotoxicity of mineral fibres observed by time-lapse video microscopy. *Toxicology*, 466, 153081. <https://doi.org/10.1016/j.tox.2021.153081>
- Fenoglio, I., Croce, A., Di Renzo, F., Tiozzo, R., & Fubini, B. (2000). Pure-silica zeolites (Porosils) as model solids for the evaluation of the physicochemical features determining silica toxicity to macrophages. *Chemical Research in Toxicology*, 13, 489–500. <https://doi.org/10.1021/tx990169u>

- Fenoglio, I., Fubini, B., Tiozzo, R., & Di Renzo, F. (2000). Effect of micromorphology and surface reactivity of several unusual forms of crystalline silica on the toxicity to a monocyte-macrophage tumor cell line. *Inhalation Toxicology*, 12, 81–89. <https://doi.org/10.1080/08958378.2000.11463233>
- Frank, A. L. (2020). Global use of asbestos - legitimate and illegitimate issues. *Journal of Occupational Medicine and Toxicology*, 15, 16. <https://doi.org/10.1186/s12995-020-00267-y>
- Garcia, J. G. N., Gray, L. D., Dodson, R. F., & Callahan, K. S. (1988). Asbestos induced endothelial cell activation and injury. *American Review of Respiratory Disease*, 138, 958–964. <https://doi.org/10.1164/ajrccm/138.4.958>
- Giordani, M., Meli, M. A., Roselli, C., Betti, M., Peruzzi, F., Taussi, M., Valentini, L., Fagiolino, I., & Mattioli, M. (2022). Could soluble minerals be hazardous to human health? Evidence from fibrous epsomite. *Environmental Research*, 206, 112579. <https://doi.org/10.1016/j.envres.2021.112579>
- Gualtieri, A. F. (2021). Bridging the gap between toxicity and carcinogenicity of mineral fibres by connecting the fibre crystal-chemical and physical parameters to the key characteristics of cancer. *Current Research in Toxicology*, 2, 42–52. <https://doi.org/10.1016/j.crttox.2021.01.005>
- Gualtieri, A. F. (2023). Journey to the centre of the lung. The perspective of a mineralogist on the carcinogenic effects of mineral fibres in the lungs. *Journal of Hazardous Materials*, 442, 130077. <https://doi.org/10.1016/j.jhazmat.2022.130077>
- Gualtieri, A. F., Gandolfi, N. B., Pollastri, S., Pollok, K., & Langenhorst, F. (2016). Where is iron in erionite? A multidisciplinary study on fibrous erionite-Na from Jersey (Nevada, USA). *Scientific Reports*, 6, 37981. <https://doi.org/10.1038/srep37981>
- Gualtieri, A. F., Lusvardi, G., Zoboli, A., Di Giuseppe, D., & Lassinanti Gualtieri, M. (2019). Biodurability and release of metals during the dissolution of chrysotile, crocidolite and fibrous erionite. *Environmental Research*, 171, 550–557. <https://doi.org/10.1016/j.envres.2019.01.011>
- Gualtieri, A. F., Pollastri, S., Bursi Gandolfi, N., & Gualtieri, M. L. (2018). In vitro acellular dissolution of mineral fibres: A comparative study. *Scientific Reports*, 8, 7071. <https://doi.org/10.1038/s41598-018-25531-4>
- Hamilton, R. F., Iyer, L. L., & Holian, A. (1996). Asbestos induces apoptosis in human alveolar macrophages. *American Journal of Physiology. Lung Cellular and Molecular Physiology*, 271, L813–L819. <https://doi.org/10.1152/ajplung.1996.271.5.L813>
- Han, S., Lemire, J., Appanna, V. P., Auger, C., Castonguay, Z., & Appanna, V. D. (2013). How aluminum, an intracellular ROS generator promotes hepatic and neurological diseases: The metabolic tale. *Cell Biology and Toxicology*, 29, 75–84. <https://doi.org/10.1007/s10565-013-9239-0>
- IARC. (2012). Arsenic, metals, fibres and dust. In *IARC Monographs on the Evaluation of Carcinogenic Risks to Humans Volume 100c*. Lyon, France: International Agency for Research on Cancer.
- Ilgren, E. B., Pooley, F. D., Larragoitia, J. C., Talamantes, M., Navarrete, G. L., Krauss, E., & Breña, A. F. (2008). First confirmed erionite related mesothelioma in North America. *Indoor and Built Environment*, 17, 567–568. <https://doi.org/10.1177/1420326X08099908>
- Jakubzick, C., Gautier, E. L., Gibbings, S. L., Sojka, D. K., Schlitzer, A., Johnson, T. E., Ivanov, S., Duan, Q., Bala, S., Condon, T., van Rooijen, N., Grainger, J. R., Belkaid, Y., Ma'ayan, A., Riches, D. W. H., Yokoyama, W. M., Ginhoux, F., Henson, P. M., & Randolph, G. J. (2013). Minimal differentiation of classical monocytes as they survey steady-state tissues and transport antigen to lymph nodes. *Immunity*, 39, 599–610. <https://doi.org/10.1016/j.immuni.2013.08.007>
- Kawanishi, S., Hiraku, Y., & Oikawa, S. (2001). Mechanism of guanine-specific DNA damage by oxidative stress and its role in carcinogenesis and aging. *Mutation Research, Reviews in Mutation Research*, 488, 65–76. [https://doi.org/10.1016/S1383-5742\(00\)00059-4](https://doi.org/10.1016/S1383-5742(00)00059-4)
- Li, M., Gunter, M. E., & Fukagawa, N. K. (2012). Differential activation of the inflammasome in THP-1 cells exposed to chrysotile asbestos and Libby “six-mix” amphiboles and subsequent activation of BEAS-2B cells. *Cytokine*, 60, 718–730. <https://doi.org/10.1016/j.cyto.2012.08.025>
- Manning, C. B., Vallyathan, V., & Mossman, B. T. (2002). Diseases caused by asbestos: Mechanisms of injury and disease development. *International Immunopharmacology*, 2, 191–200. [https://doi.org/10.1016/S1567-5769\(01\)00172](https://doi.org/10.1016/S1567-5769(01)00172)
- Mantovani, A., Sica, A., Sozzani, S., Allavena, P., Vecchi, A., & Locati, M. (2004). The chemokine system in diverse forms of macrophage activation and polarization. *Trends in Immunology*, 25, 677–686. <https://doi.org/10.1016/j.it.2004.09.015>
- Mirata, S., Almonti, V., Di Giuseppe, D., Fornasini, L., Raneri, S., Vernazza, S., Bersani, D., Gualtieri, A. F., Bassi, A. M., & Scarfi, S. (2022). The acute toxicity of mineral Fibres: A systematic in vitro study using different THP-1 macrophage phenotypes. *International Journal of Molecular Sciences*, 23, 2840. <https://doi.org/10.3390/ijms23052840>
- Nackerdien, Z., Kasprzak, K. S., Rao, G., Halliwell, B., & Dizdaroglu, M. (1991). Nickel (II)- and cobalt (II)-dependent damage by hydrogen peroxide to the DNA bases in isolated human chromatin. *Cancer Research*, 51, 5837–5842.
- Nicolini, F., Bocchini, M., Bronte, G., Delmonte, A., Guidoboni, M., Crinò, L., & Mazza, M. (2020). Malignant pleural mesothelioma: State-of-the-art on current therapies and promises for the future. *Frontiers in Oncology*, 9, 1519. <https://doi.org/10.3389/fonc.2019.01519>
- Ollikainen, T., Linnainmaa, K., & Kinnula, V. L. (1999). DNA single strand breaks induced by asbestos fibers in human pleural mesothelial cells in vitro. *Environmental and Molecular Mutagenesis*, 33, 153–160. [https://doi.org/10.1002/\(SICI\)1098-2280\(1999\)33:2<153::AID-EM7>3.0.CO;2-Q](https://doi.org/10.1002/(SICI)1098-2280(1999)33:2<153::AID-EM7>3.0.CO;2-Q)
- Pacella, A., Andreozzi, G. B., Nodari, L., & Ballirano, P. (2019). *Chemical and structural characterization of UICC crocidolite fibres from Koegas, mine. Periodico di Mineralogia* 88.
- Pollastri, S., Gualtieri, A. F., Vigliaturo, R., Ignatyev, K., Strafella, E., Pugnali, A., & Croce, A. (2016). Stability of mineral fibres in contact with human cell cultures. An in situ μ XANES, μ XRD and XRF iron mapping study. *Chemosphere*, 164, 547–557. <https://doi.org/10.1016/j.chemosphere.2016.08.139>
- Puhakka, A., Ollikainen, T., Soini, Y., Kahlos, K., Säily, M., Koistinen, P., Pääkkö, P., Linnainmaa, K., & Kinnula, V. L. (2002). Modulation of DNA single-strand breaks by intracellular glutathione in human lung cells exposed to asbestos fibers. *Mutation Research, Genetic Toxicology and Environmental Mutagenesis*, 514, 7–17. [https://doi.org/10.1016/S1383-5718\(01\)00322-9](https://doi.org/10.1016/S1383-5718(01)00322-9)
- Rao, J., & Otto, W. R. (1992). Fluorimetric DNA assay for cell growth estimation. *Analytical Biochemistry*, 207, 186–192. [https://doi.org/10.1016/0003-2697\(92\)90521-8](https://doi.org/10.1016/0003-2697(92)90521-8)
- Richter, E., Ventz, K., Harms, M., Mostertz, J., & Hochgräfe, F. (2016). Induction of macrophage function in human THP-1 cells is associated with rewiring of MAPK signaling and activation of MAP 3K7 (TAK1) protein kinase. *Frontiers in Cell and Developmental Biology*, 4, 21. <https://doi.org/10.3389/fcell.2016.00021>
- Røe, O. D., & Stella, G. M. (2015). Malignant pleural mesothelioma: History, controversy and future of a manmade epidemic. *European Respiratory Review*, 24, 115–131. <https://doi.org/10.1183/09059180.00007014>
- Salnikow, K., Su, W., Blagosklonny, M. V., & Costa, M. (2000). Carcinogenic metals induce hypoxia-inducible factor-stimulated transcription by reactive oxygen species-independent mechanism. *Cancer Research*, 60, 3375–3378.
- Sarkar Phyllis, A. K., Tortora, G., & Johnson, I. (2021). *The Fairchild books dictionary of textiles*. Fairchild Books. <https://doi.org/10.5040/9781501365072>

- Thyssen, G. M., Keil, C., Wolff, M., Sperling, M., Kadow, D., Haase, H., & Karst, U. (2018). Bioimaging of the elemental distribution in cocoa beans by means of LA-ICP-TQMS. *Journal of Analytical Atomic Spectrometry*, 33, 187–194. <https://doi.org/10.1039/C7JA00354D>
- Treadwell, M. D., Mossman, B. T., & Barchowsky, A. (1996). Increased neutrophil adherence to endothelial cells exposed to asbestos. *Toxicology and Applied Pharmacology*, 139(1), 62–70. <https://doi.org/10.1006/taap.1996.0143>
- Vandesompele, J., De Preter, K., Pattyn, F., Poppe, B., Van Roy, N., De Paepe, A., & Speleman, F. (2002). Accurate normalization of real-time quantitative RT-PCR data by geometric averaging of multiple internal control genes. *Genome Biology*, 3, research0034. <https://doi.org/10.1186/gb-2002-3-7-research0034>
- Wang, H., & Joseph, J. A. (1999). Quantifying cellular oxidative stress by dichlorofluorescein assay using microplate reader. Mention of a trade name, proprietary product, or specific equipment does not constitute a guarantee by the United States Department of Agriculture and does not imply its approval to the exclusion of other products that may be suitable. *Free Radical Biology and Medicine*, 27, 612–616. [https://doi.org/10.1016/S0891-5849\(99\)00107-0](https://doi.org/10.1016/S0891-5849(99)00107-0)
- World Health Organization (WHO). (2014). Chrysotile asbestos. <https://www.who.int/publications/m/item/who-workshop-on-mechanisms-of-fibre-carcinogenesis-and-assessment-of-chrysotile-asbestos-substitutes>

How to cite this article: Almonti, V., Vernazza, S., Mirata, S., Tirendi, S., Passalacqua, M., Gualtieri, A. F., Di Giuseppe, D., Scarfi, S., & Bassi, A. M. (2024). Toxicity and inflammatory potential of mineral fibres: The contribute of released soluble metals versus cell contact direct effects. *Journal of Applied Toxicology*, 44(8), 1166–1183. <https://doi.org/10.1002/jat.4610>